

Thermodynamic and kinetic aspects of RNA pulling experiments

M. Mañosas and F. Ritort

Departament de Fisica Fonamental, Universitat de Barcelona,
Diagonal 647, 08028 Barcelona, Spain

March 2, 2019

Abstract

Recent single-molecule pulling experiments have shown how it is possible to manipulate RNA molecules using optical tweezers force microscopy. We investigate a minimal model for the experimental setup which includes a RNA molecule connected to two polymers (handles) and a bead, trapped in the optical potential, attached to one of the handles. Initially, we focus on small single-domain RNA molecules which unfold in a cooperative way. The model qualitatively reproduces the experimental results and allow us to investigate the influence of the bead and handles on the unfolding reaction. A main ingredient of our model is to consider the appropriate statistical ensemble and the corresponding thermodynamic potential describing thermal fluctuations in the system. We then investigate several questions relevant to extract thermodynamic information from the experimental data. Next, we study the kinetics using a dynamical model. Finally, we address the more general problem of a multidomain RNA molecule with Mg^{2+} -tertiary contacts that unfolds in a sequential way and propose techniques to analyze the breakage force data in order to obtain the reliable kinetics parameters that characterize each domain.

1 Introduction

The RNA molecule plays a central role in molecular biology showing an enzymatic function during the translation and splicing processes [1, 2]. Experiments based on the manipulation of single-biomolecules, such as laser tweezers force microscopy, allow scientists to investigate their mechanical properties. These give information about the structure, stability and the interactions involved in the formation of such structures [3, 4, 5, 6, 7, 8, 9]. In these experiments mechanical force is applied to the ends of a RNA molecule. The molecule is then pulled [10, 11] until a value of the force is reached such that the molecule unfolds. If the pulling process is reversed then the molecule refolds again. In these experiments the force exerted upon the system is recorded as a function of the end-to-end distance giving the so-called force-extension curve (FEC). The nature of this unfolding-refolding process is stochastic and therefore the values of the force at which the molecule unfolds-refolds change from experiment to experiment. Sometimes, as in the case of presence of Mg^{2+} -tertiary contacts, it is not possible to pull the molecule in quasi-static conditions because the relaxation time is too large for the experimental possibilities which are largely limited due to the presence of strong drift effects in the machine. Therefore, during the pulling process, the molecule is driven to a non-equilibrium state which is characterized by strong irreversibility effects. The study of this pulling process might be useful to understand many biological processes where biomolecules are unfolded under locally applied force, for example when the mRNA goes through the ribosome during the translation process.

To manipulate a RNA molecule some synthesized polymers typically several hundred nanometers long (called handles) have to be chemically linked to the extremes of the RNA molecule. A polystyrene bead is then chemically attached to the end of

one of these handles and used to measure the force by reading its position inside the optical trap. These additional elements (bead and handles) are an inseparable part of any pulling experiment and they have an influence on the unfolding process. To characterize the thermal behavior of the pulled global system (bead, handles plus RNA molecule) it is important to identify the proper control parameter. This is an essential step towards the modelization of the experiment and has several consequences. For instance, the force acting on the extremes of the RNA molecule cannot be externally controlled but fluctuates and its mean value depends in a non-linear way on the value of the control parameter. The control parameter determines the relevant thermodynamic potential defining the equilibrium state of the global system as well as the magnitude of the fluctuations around that state. A proper inclusion of these parts is necessary to accurately interpret the experimental data. Another important point of the work is the model for the RNA molecule. We consider the RNA molecule to be composed by different domains, each one showing cooperative unfolding. Each domain is then modeled as a two-states system: the unfolded state (UF) and the folded one (F), which are separated by a kinetic barrier. A main effort throughout this paper is to present in the most clear way the appropriate theoretical frame to understand pulling experiments leaving aside further additional complications, nevertheless important, such as a detailed response of the optical tweezers machine or the microscopic structure of the RNA molecule.

The goal of this paper is twofold: (i) we show how to build a minimal model aiming to reproduce the experimental setup including all the aforementioned elements (bead, handles and the RNA molecule) and quantitatively reproducing various experimental results; (ii) we show how to analyze experimental data extracted from both quasi-static and out-of-equilibrium pulling experiments in order to obtain thermodynamic and kinetic information about the unfolding reaction.

The paper is divided into three main parts. In the first part of the paper (Sections 2,3,4) we describe the model for the experimental setup (Sec. 2) and introduce the ensemble that is relevant to model the pulling experiment (Sec. 2.1). In Sec. 3 we describe the two-states model convenient to reproduce the cooperative unfolding of the RNA molecule and in Sec. 4 we describe the models used for the bead and handles. In the second part of the paper (Sections 5,6) we analyze the unfolding-refolding behavior of a cooperative two-states RNA molecule in a pulling experiment for both equilibrium and non-equilibrium regimes. For the equilibrium regime, we compute the partition function in the ensemble that is experimentally relevant, and derive an expression for the quasi-static work exerted upon the system as the molecules unfolds. This expression relates the work measured in a quasi-static pulling process to the difference of free energy between the F and UF states at zero force ΔG^0 . We analyze in detail the different thermodynamic contributions to the total work, the influence of the parameters describing bead and handles on the FEC, and obtain expressions for the force at the midpoint of the transition. For the non-equilibrium behavior we investigate in detail the fraction of molecules that unfold (refold) more than once during the unfolding (refolding) path, which is a quantity amenable to experimental checks. We find that this fraction is related to the mean dissipated work exerted upon the system, which gives us a way to extract the reversible work in non-equilibrium processes just by measuring the total work. We also identify an interesting symmetry property relating these fractions for the forward and reverse processes. To endorse most of our theoretical results we also consider a simulation of a pulling experiment that allow us to obtain the characteristic FEC, either in a situation where the transition occurs in equilibrium or in a situation where it does not. In the third part of the paper (Sec. 7), we address the unfolding behavior of complex RNA molecules with more than one folded-domain and in the presence of Mg^{2+} -dependent barriers. In this case, the refolding is not observed at the experimental conditions, and the distribution of the breakage force is a first order Markov process [12, 13]. We focus our attention in the specific case of RNA molecules where domains unfold in a sequential fashion according to a reproducible path. This unfolding mechanism is generally a consequence of the topological connectivity of the different parts of the molecule and of the blockade of the force induced by the most external tertiary contacts on the interior domains. We model the molecule as a series of domains, each represented

by a two-states system, and we compute the distribution of breakage force for each domain. We propose several methods of analyzing the breakage force data in order to achieve reliable values for the height and position of the barrier of each domain. In Sec. 8 we present the conclusions. Five appendixes are devoted to describe some analytical calculations.

2 Model for the experimental setup

We consider a minimal model in order to reproduce the experimental setup of a pulling experiment carried out using laser tweezers force microscopy [10, 14]. The model (Fig. 1) is composed by a small RNA molecule connected to two polymers called handles¹ which are used to attach the small RNA molecule to two beads at each end. One bead is confined in the optical trap generated by the laser beams, the other is held fixed to the tip of a micropipette by air suction.

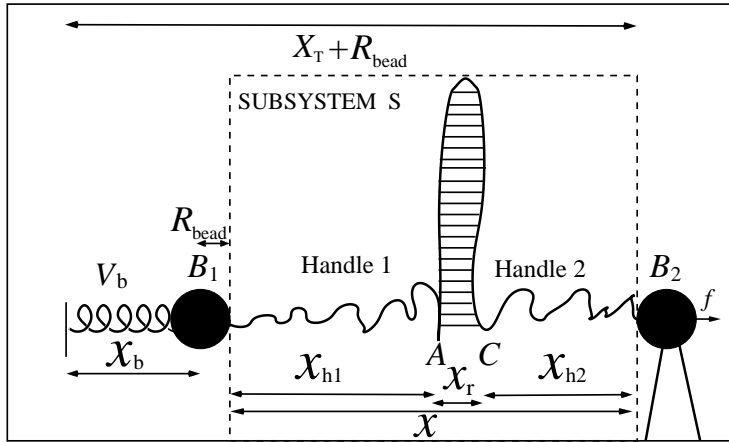


Figure 1: Schematic picture of the model for the experimental setup in a RNA pulling experiment as described in the text. We show the configurational variables of the system x_b, x_r, x_{h1}, x_{h2} which are the projections of the end-to-end distance of each element along the reaction coordinate axis (i.e. the axis along which the force is applied). The potential $V_b(x_b)$ is well described by an harmonic potential of one-dimensional spring with rest position at $x_b = 0$.

The whole system consists of a chain of connected elements. Starting from the left side of the chain there is a bead (B_1) of radius R_{bead} that is trapped in the laser tweezers potential, $V_b(x)$ ². We use the position of this bead B_1 to read the force acting on the system in the same way as the needle of a 'manometer' is used to read the pressure exerted by a gas on the walls of a container³. The second element is a handle (handle 1) with one end specifically attached to the bead B_1 and the other end attached to the RNA molecule at the point A . The second handle (handle 2) has one end specifically attached to the RNA molecule at the point C . The other end is specifically attached to the bead B_2 , fixed to the tip of a micropipette. The molecule is pulled by moving the micropipette along the x direction. The configurational variables of this simplified system are taken as the projections of the end-to-end distances of each element along the force axis: $x_{h1} = \overline{B_1 A} - R_{\text{bead}}$, $x_{h2} = \overline{C B_2} - R_{\text{bead}}$ for the distances of the handles, $x_r = \overline{A C}$ for the RNA end-to-end distance and x_b for the

¹These are hybrids of DNA and RNA rather than single stranded DNA or RNA polymers in order to avoid the formation of secondary structures

²Although the trap potential should be defined in the three-dimensional space $V_b(\vec{x})$ we will consider $V_b(x)$ as the potential of mean-force projected along the reaction coordinate axis. This approximation is very accurate as fluctuations along the y, z directions are assumed to hardly affect the unfolding behavior of the RNA molecule.

³This is not the way the force is usually measured in dual beam optical tweezers where two photodetectors located at opposite sides of the chamber are used to collect the total amount of deflected light which is then converted into force after calibration of the machine.

position of the bead B_1 in the trap. The force f is measured by reading the position x_b of the bead B_1 :

$$f = \left| \frac{dV_b(y)}{dy} \right|_{y=x_b}. \quad (1)$$

We define the subsystem S as that composed by the two handles and the small RNA molecule. The end-to-end distance for the subsystem S is then given by $x = x_{h_1} + x_{h_2} + x_r$ (Fig. 1). The total distance between the center of the trap and the tip of the micropipette is given by $X_T + R_{\text{bead}} = x_b + x + R_{\text{bead}}$. Pulling experiments give FECs, $f(x)$, corresponding to the force exerted on the chain (1) measured through the position of the bead B_1 as a function of the end-to-end distance of subsystem S .

2.1 Ensembles

Experimentally it is possible to consider two different ensembles depending on which variable is used as the externally imposed non-fluctuating parameter ⁴.

- **Mixed ensemble:** The total distance between the center of the trap and the tip of the micropipette is held fixed, hence X_T is the externally controlled parameter. In this ensemble there are fluctuations in x and f given by [16, 17],

$$\langle \delta x^2 \rangle = \frac{k_B T}{k_x(X_T) + k_b(X_T)}, \quad \langle \delta f^2 \rangle = \frac{k_B T k_b^2}{k_x(X_T) + k_b(X_T)},$$

with $k_x(X_T) = \frac{d\langle f \rangle}{d\langle x \rangle} \Big|_{X_T}$, $k_b(X_T) = \frac{d\langle f \rangle}{d\langle x_b \rangle} \Big|_{X_T}$, (2)

where $\langle \dots \rangle$ stands for thermal average, k_B is the Boltzmann constant, T is the temperature of the bath, $k_b(X_T)$ is the stiffness of the optical trap and $k_x(X_T)$ is the effective rigidity corresponding to the subsystem S . The latter is determined by the serial compliance

$$k_x(X_T) = \left[\frac{1}{k_{h_1}(X_T)} + \frac{1}{k_{h_2}(X_T)} + \frac{1}{k_r(X_T)} \right]^{-1}, \quad (3)$$

where k_{h_i} ($i = 1, 2$) and k_r are the rigidities of the handles 1, 2 and the RNA respectively. These rigidities are X_T dependent and so are the fluctuations (2).

- **Force ensemble:** In this case a piezo actuator controls the force (and therefore the position of the bead B_1). In this ensemble X_T and x are fluctuating variables, $\langle \delta X_T^2 \rangle = \langle \delta x^2 \rangle = k_B T / k_x(f)$, where $k_x(f)$ is the stiffness of the subsystem S when the force is held fixed, $k_x(f) = \left[\frac{d\langle x \rangle}{df} \right]^{-1}$.

Most of the theoretical work for the denaturation of RNA in pulling experiments considers the force ensemble. However, it is experimentally very difficult to work in the force ensemble where either the force or the variable x_b must be controlled. Indeed, for X_T to fluctuate the center of the trap must also fluctuate to compensate for the fluctuations in the force. It is difficult to imagine how to experimentally implement such ensemble. Therefore the most natural ensemble is that where X_T is constant. Indeed this is the ensemble most relevant for the experiments and therefore we will work in the mixed ensemble throughout this article.

3 Two-states model for a single RNA domain under the effect of an external mechanical force

The unfolding of some biomolecules under the effect of a mechanical force is a highly cooperative process that can be qualitatively described by a two-states model. The two-states model has a long tradition in physics and has been applied previously by several authors in order to explain the unfolding behavior of single domains of proteins

⁴The existence of an external non-fluctuating parameter is required to have a well defined equilibrium state.

and RNA hairpins [10, 18, 19, 20, 21, 22]. Recently, it has been shown how such a simple phenomenological description, with Kramer transitions-rates, does not fully reproduce the kinetics observed in pulling experiments of the protein Titin, and more realistic descriptions have been proposed [23].

Let us consider an RNA molecule isolated from the rest of the system in equilibrium at constant temperature, pressure and zero force. In the simplest description both states (hereafter denoted by UF -unfolded- and F -folded-) are characterized by their Gibbs free energy G_{UF}^0 and G_F^0 respectively and the RNA molecule occupies each state with a probability given by the Boltzmann distribution. In a more refined description the molecule can also occupy intermediate configurations depending on the number n of the first-opened, or denatured, bases (Fig. 2 (a)) [24]. The F and UF states correspond then to the RNA configuration with $n = 0$ and $n = N$ bases opened, where N is the total number of pair of bases of the molecule. The free energy landscape is described by a function $G^0(n)$ which characterizes the probability of a hairpin having the first n bases opened (Fig. 2 (b)). This description excludes the existence of other *breathing* intermediate configurations that might be relevant for the unfolding reaction [25].

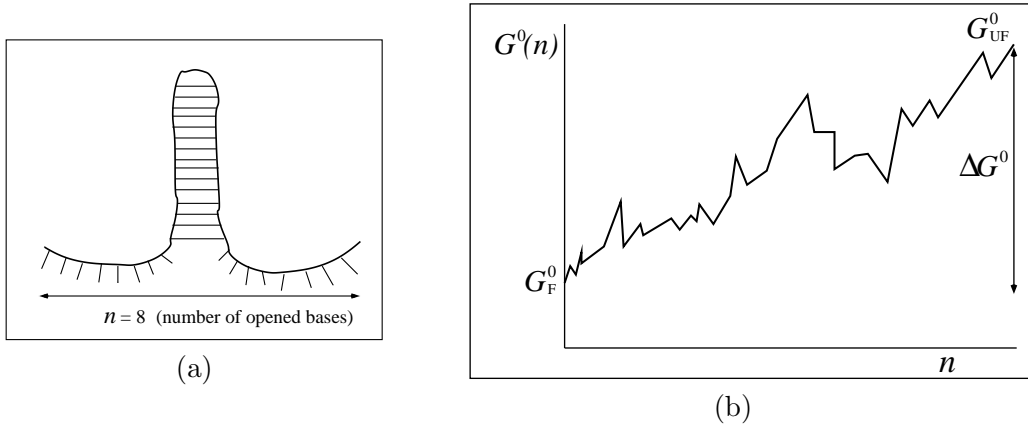


Figure 2: Schematic representation of (a) a RNA hairpin with $n = 8$ bases opened. (b) the free energy landscape for a single RNA hairpin at zero force as a function of the number of denatured bases n at $T < T_{\text{melting}}$ (melting temperature of the RNA) and normal ionic conditions. In this situation the stable state is the folded one with $n = 0$.

When an externally controlled force f is applied to the ends of the RNA molecule the adequate thermodynamic potential to consider is the Legendre transform of the Gibbs free energy $G'(n) = G^0(n) - fx_r(n)$ [26]. The free energy landscape G' is then tilted along the reaction coordinate x_r , which is the projection of the end-to-end distance of the molecule in the axis force and explicitly depends on the number of opened bases n . Since we work in the ensemble where neither f nor x_r are control parameters the non-fluctuating parameter X_T determines the adequate thermodynamic potential G_{X_T} . The free energy G_{X_T} of the system shown in Fig. 1 is a potential of a mean force that characterizes the equilibrium state of the whole system, including the handles, the bead and the RNA molecule, at fixed value of X_T . In order to build the model is useful to represent the free energy G_{X_T} , as a function of the end-to-end distance of the subsystem S , as shown in Fig. 3 (a). This picture tells us about the probability $p_{X_T}(x)$ of finding the subsystem S at a given value of its end-to-end distance x for a fixed value of X_T , $p_{X_T}(x) \propto \exp(-\beta G_{X_T}(x))$, where $\beta = 1/k_B T$.

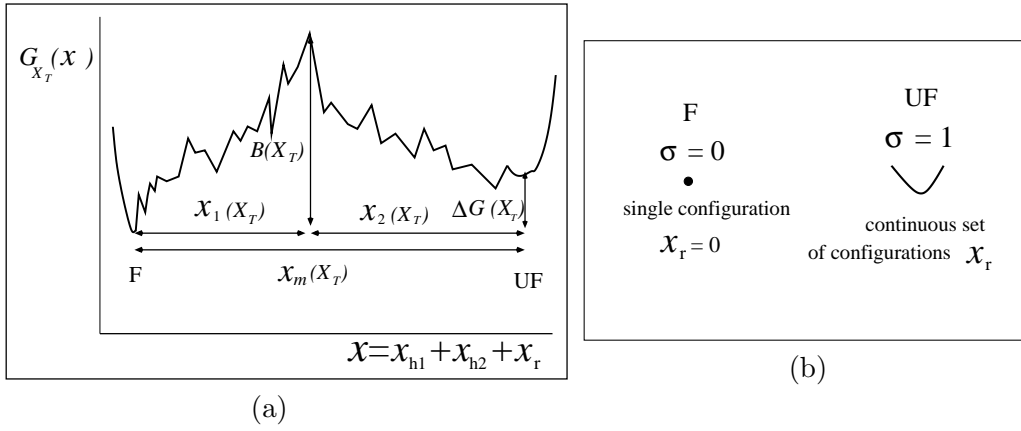


Figure 3: (a) Schematic representation of the free energy landscape $G_{X_T}(x)$ for the whole system at $T < T_{\text{melting}}$, for $X_T < X_T^c$ (where X_T^c is the value of X_T where both states F and UF are equiprobable) and normal ionic conditions. In this situation the stable state is still the folded one. We also show all the parameters characterizing the two states model. (b) Schematic representation of the relevant configurations in the F and UF states along the reaction coordinate x_r . We consider the F state to be characterized by a single configuration $x_r = 0$ and the UF state by a continuous set of values of x_r . We use the label $\sigma = 0$ for the F state and $\sigma = 1$ for the UF state.

The free energy landscape $G_{X_T}(x)$ shows two pronounced minima corresponding to the F and UF states (Fig. 3). The discrete variable σ stands for the state of the domain: the value $\sigma = 0$ denotes the F state and $\sigma = 1$ the UF state. The relative thermodynamic stability of these states depends on the difference of free energy between them, $\Delta G(X_T)$. Moreover we will consider the existence of an intermediate or transition state along the reaction path from the F to the UF states and vice versa. This transition state is the intermediate RNA state with highest free energy connecting the F and the UF state along the reaction path. It may correspond to a RNA configuration where the first $n = n^*$ bases are opened⁵. In the simplest scenario the intermediate state can be assumed to have a very short lifetime, its main effect is to hinder transitions from the F to the UF state and back. In this scenario the transition state can be represented by an activation barrier and this is the model we will adopt throughout the paper. The F and UF states are separated by a barrier of height $B(X_T)$ measured relative to the F state. The barrier is located at a distance $x_1(X_T)$ from the F state and $x_2(X_T)$ from the UF state. The distance between the two states is $x_m(X_T) = x_1(X_T) + x_2(X_T)$. Because the rigidity of the RNA molecule in the F state is very large we can assume this state to be characterized by a single configuration corresponding to the value $x_r = 0$ of the reaction coordinate; fluctuations around this configuration cost so much energy that they are highly improbable. The RNA in the UF state has a finite rigidity, hence it is represented by a set of configurations within a continuous range of values of x_r (Fig. 3 (b)).

4 Modeling the different parts of the setup

In this section we specify how we model the different elements of the system: the bead trapped in the optical tweezers potential, the two handles, and the RNA.

⁵We stress that the shape of the free energy landscape depends on X_T as well as the location of the barrier corresponding to the intermediate state. Therefore the value of n^* that characterizes the transition state is also X_T dependent. There are experimental limitations to follow the folding and unfolding of the molecule (hopping) given by the operational range of frequencies of the instrument used. For instance, in [10] this operational range was 0.05 – 20Hz, meaning that hopping events out of this range were not observable. Moreover, in pulling processes the folding-unfolding reaction only occurs in a narrow range of values of the control parameter X_T around X_T^c , otherwise the folding-unfolding relaxation time is too large. Hence the study of the folding-unfolding kinetics is restricted to the regime $X_T \approx X_T^c$ and to the operational range of frequencies. Therefore, as the transition state n^* is only relevant for the study of the kinetics, we assume n^* independent of X_T , $n^* = n^*(X_T^c)$.

4.1 Model for optical tweezers: a bead matched to a spring

Typical experimental values for the trap stiffness and the diameter of the beads are $k_b \approx 0.15 - 0.05 \text{ pN/nm}$ and $R_{\text{bead}} \approx 1 - 3 \mu\text{m}$ respectively. We consider that the bead follows a Langevin dynamics of an overdamped particle (i.e. without inertial term)⁶ :

$$\gamma \frac{dx_b}{dt} = F_R(x_b) + \xi(t) , \quad (4)$$

where γ is the friction coefficient and F_R is the resultant force applied to the bead. The stochastic term $\xi(t)$ is a white noise with mean value $\langle \xi(t) \rangle = 0$ and variance $\langle \xi(t)\xi(t') \rangle = 2k_B T \gamma \delta(t - t')$. The force F_R has two contributions: one coming from the optical trap potential, f , given by (1), and the other from the subsystem S , f_x ⁷. Therefore $F_R = -f + f_x(x_b)$. The experimental results [10, 11] show a linear dependence of the force f on x along the transition (rip) where the variable x refers to the subsystem S (Fig. 1), hence we conclude that the optical trap V_b is well modeled by an harmonic potential of stiffness k_b . We can then express the force f measured through the optical tweezers as $f = k_b x_b = k_b(X_T - x)$, where we have used (1). In equilibrium the average force acting upon the bead is zero $\langle F_R \rangle$, hence $\langle f_x \rangle = k_b \langle x_b \rangle$. However x_b fluctuates and so both instantaneous forces f and f_x are not identical. Doing an expansion around the equilibrium position of the bead, x_{eq} ⁸, we obtain:

$$\gamma \frac{dx_b}{dt} = -k_R(x_b - x_{eq}) + \xi(t) , \quad (5)$$

where k_R is the effective spring constant applied to the bead, $k_R = k_x + k_b$, with k_x given by (3). The relaxation time of the system (i.e the typical time during which the position of the bead decorrelates), τ_b , is given by $\tau_b = \gamma/k_R$. Applying the Stokes's law for the friction coefficient in water we obtain: $\gamma = 6\pi R \eta \approx 10^{-5} \text{ pNs/nm}$. The stiffness of the handles and the RNA are force dependent. Near the F-UU transition, typically these stiffness values are, at least, one order of magnitude bigger than k_b . Taking $k_b = 0.1 \text{ pN/nm}$, and $k_{h_1}, k_{h_2}, k_\sigma > 1 \text{ pN/nm}$ we get $\tau_b < 10^{-5} \text{ s}$ ⁹. By collecting data at frequencies smaller than 10^5 Hz we can guarantee that we will not have effects due to the bead's overdamping, hence the bead relaxes quickly to its new equilibrium position at each step. This ensures that assuming an instantaneous relaxation of the bead position is enough to capture its overdamped dynamics.

4.2 Polymer model for handles and single-stranded RNA

The handles and the single-stranded RNA (ssRNA), the UF state of the RNA, are polymers that typically measure $d \approx 1 - 3 \text{ nm}$ in diameter and $L \approx 20 - 500 \text{ nm}$ in length. As the bead has a much bigger size than the polymers the friction coefficient (and therefore the relaxation time) for the polymers is much smaller. This allows us (as we do for the bead) to only consider an instantaneous relaxation for the handles and the ssRNA. To describe the equilibrium behavior of the handles and the ssRNA under the effect of an external force we use the worm-like-chain (WLC) model [27]. This is described by a Hamiltonian that includes a local bending term as well as the potential energy of the polymer in the presence of the pulling force. Parameterizing the polymer with the arc length s , the energy function can be written as:

$$E_{WLC} = \int_0^{L_o} \left[\frac{k_B T P}{2} \left(\frac{d\vec{t}(s)}{ds} \right)^2 - f \cos \theta(s) \right] ds , \quad (6)$$

⁶In (4) we are neglecting the drag force felt by the bead (equal to $-\gamma v$) as the chamber is moved (and the water dragged relative to the lab frame) at a certain pulling speed $v = \frac{dX_T}{dt}$. For the range of pulling speeds used in the experiments this contribution is negligible, of the order of 0.1 pN .

⁷This is also the force exerted upon the subsystem S for a given value of $x = X_T - x_b$.

⁸We expand f_x and f around x_{eq} keeping only the first term in $(x_b - x_{eq})$, i.e $f_x \approx \langle f_x \rangle + k_x(x_{eq} - x_b)$, with k_x given by (3), and $f \approx \langle f \rangle + k_b(x_b - x_{eq})$. This approximation is valid in the regime where the force fluctuations are not big. Using that at equilibrium $\langle f \rangle = \langle f_x \rangle$ we obtain $F_R = -f + f_x \approx -(k_x + k_b)(x_b - x_{eq})$.

⁹In absence of handles $k_R = k_b$ and $\tau_b = 10^{-3} \text{ s}$. Therefore 10^{-3} s is the slowest relaxation time for the bead corresponding to the regime where the handles have practically no rigidity, $k_x \approx 0$, a situation only encountered at small forces (below 1 pN approximately).

where L_o is the contour length of the polymer, $\vec{t}(s)$ is the unit tangent vector along s , $\theta(s)$ is the angle between $\vec{t}(s)$ and the force axis, and P is the persistence length defined as the typical distance over which \vec{t} -correlations decay to zero: $\langle \vec{t}(s)\vec{t}(s') \rangle \approx e^{-\frac{|s-s'|}{P}}$. The persistence length of a polymer depends on the ionic conditions [28], and typical values are 50nm for double-stranded DNA (dsDNA) and 1nm for ssRNA. The thermodynamic properties of this model cannot be exactly computed, yet there are useful extrapolation formulas. Bustamante et al. [29] have proposed a simple expression for the force as a function of mean end-to-end distance of the polymer x ,

$$f = \frac{k_B T}{P} \left[\frac{1}{4(1-x/L_o)} - 1/4 + x/L_o \right]. \quad (7)$$

Eq.(7) gives the exact solution as x approaches either zero or L_o and is accurate at least up to 90% in between. Bouchiat et al. [30] have given an expression with an accuracy of 99% by adding to (7) a polynomial of seventh order. The WLC model works well only at low forces, in the so called entropic regime where the molecule behaves as an entropic spring. At high forces there is an enthalpic correction due to the fact that the bonds are stretched and the contour length L_o increases. To incorporate this effect it is then enough to replace x/L_o by $x/L_o - f/E_y$ in (7), where E_y is the Young modulus of the polymer (typical values are $E_y \approx 500 - 1500$ pN for DNA-RNA molecules).

Throughout Secs. 5 and 6 we analyze the unfolding dynamics and thermodynamics of a single hairpin of RNA aiming to reproduce the results obtained from a pulling experiment for the hairpin P5ab in 10mM Mg^{2+} [10]. In Sec. 5 we use the partition function analysis to individuate the different thermodynamic contributions to the total free energy or reversible work done upon the system. Next in Sec. 6 we do numerical simulations of a pulling experiment.

5 Thermodynamic analysis

In this section we use the tools of statistical mechanics to analyze the thermodynamics of the system represented in Fig. 1. Most of the analytical development is done in appendix A and in Sec. 5.1 we give the main results. In Sec. 5.2 we show how to get the force-extension curve (FEC), the value of the force at the midpoint of the F-UF transition F^c , and the different contributions to the total reversible work coming from the different elements of the system. In Sec. 5.3 we derive an expression that relates the reversible work exerted upon the subsystem S across the transition with the difference of free energy between the F and UF states at zero force, ΔG^0 . As this is an experimentally measurable quantity this procedure provides a way to estimate the unfolding free energy of the molecule, a quantity biologically relevant as it determines the fate of biochemical reactions. Finally in Sec. 5.4 we show how to apply these relations to a specific example.

5.1 Definitions

In equilibrium the observables x_α and the conjugated forces f_α with $\alpha = h_1, h_2, r, b$ (referring to the different elements, handle 1 and 2, RNA and bead respectively) fluctuate. However, the thermodynamic free energy is only a function of the mean values of these observables that we denote by $\langle x_\alpha \rangle$, $\langle f_\alpha \rangle$. A representation of $\langle f_\alpha \rangle$ versus $\langle x_\alpha \rangle$ gives what we call the thermodynamic force extension curve (TFEC) for the element α in the mixed ensemble. If α refers to the whole subsystem S then the TFEC corresponds to the usual force-extension recorded in RNA pulling experiments, assuming that the pulling process is carried out reversibly. We can also define the restricted average $\langle \mathcal{O} \rangle_\sigma(X_T)$ as the mean value of the observable \mathcal{O} when the RNA molecule is in the state σ for a fixed total end-to-end distance X_T . From now on, all the dependencies of the observables on the variable X_T will not be explicitly written, hence $\langle \mathcal{O} \rangle_\sigma(X_T) \equiv \langle \mathcal{O} \rangle_\sigma$. In appendix A we derive an expression for the partition function $Z(X_T)$, corresponding to the system schematically represented in Fig. 1. Applying the saddle point technique, and separating the contributions that come from the F

$(\sigma = 0)$ and UF $(\sigma = 1)$ states we get:

$$Z(X_T) = Z_0(X_T) + Z_1(X_T), \quad (8)$$

where

$$Z_0(X_T) \approx \exp \left[-\beta \left(W_{h_1}(\langle x_{h_1} \rangle_0) + W_{h_2}(\langle x_{h_2} \rangle_0) + V_b(\langle x_b \rangle_0) \right) \right], \quad (9)$$

$$Z_1(X_T) \approx \exp \left[-\beta \left(W_{h_1}(\langle x_{h_1} \rangle_1) + W_{h_2}(\langle x_{h_2} \rangle_1) + V_b(\langle x_b \rangle_1) + \Delta G^0 + W_r(\langle x_r \rangle_1) \right) \right]. \quad (10)$$

Here V_b represents the optical trap potential and ΔG^0 is the free energy difference between the F and the UF states at zero force. The function $W_\alpha(x)$ corresponds to the reversible work performed by adiabatically stretching the element α from $x_\alpha = 0$ to $x_\alpha = x$ and it is given by

$$W_\alpha(x_\alpha) = \int_0^{x_\alpha} dx f_\alpha(x), \text{ with } \alpha = h_1, h_2, r, \quad (11)$$

where $f_\alpha(x)$ is the TFEC for the element α (see appendix A). We can define the probabilities for the RNA molecule of being in the F and the UF states by p_0 and p_1 respectively,

$$p_\sigma(X_T) = \frac{Z_\sigma(X_T)}{Z(X_T)}, \text{ with } \sigma = 0, 1. \quad (12)$$

The thermodynamic value of any observable \mathcal{O} can be expressed in terms of these probabilities,

$$\langle \mathcal{O} \rangle = p_0 \langle \mathcal{O} \rangle_0 + p_1 \langle \mathcal{O} \rangle_1. \quad (13)$$

At the midpoint of the transition both states are equally probable,

$$p_0(X_T^c) = p_1(X_T^c) \text{ or } Z_0(X_T^c) = Z_1(X_T^c), \quad (14)$$

where these functions have been defined in (9,10) and (12). Hence the midpoint of the transition in the mixed-ensemble is defined by the value of the control parameter X_T^c that verifies (14).

5.2 Computation of the transition force F^c , the TFEC and the different contributions to the reversible work.

The force at the transition, F^c , is computed as the mean value of the force at X_T^c given by (14). To reproduce the experimental results obtained for the P5ab RNA molecule in 10mM Mg^{2+} [10] we use the parameters given by Tables 1 and 2 getting $F^c = 15.2$ pN¹⁰. This value is close to the one reported from the experiments $F_{\text{exp}}^c = 14.5 \pm 1$ pN [10]. We also verify that the force at the transition F^c is quite stable with respect to changes in the parameters of the problem used to model the handles and the bead trapped in the optical potential, such as the persistence and contour length of the handles, the spring constant and the bead radius. However, as the value of F^c is highly influenced by the characteristics of the RNA molecule, we conclude that the dependence of the value of F^c with the system is basically through the quantities ΔG^0 , L_r and P_r .

$k_B T$ [pNnm]	k_b [pN/nm]	$P_{h_1} = P_{h_2}$ [nm]	$L_{h_1} = L_{h_2}$ [nm]	$E_y^{h_1} = E_y^{h_2}$ [pN]
4.14	0.1	10	160	1000

Table 1: Summary table of the parameter values used to model the handles and the bead in the optical trap. We use the value for the Young modulus corresponding to a dsDNA. The value for the other parameters have been taken from [10].

¹⁰In our model we are considering the F state to be localized at $x_r = 0$. However also the folded RNA has an end-to-end distance d_r (the diameter of the hairpin) that tends to be aligned along the force axis when the force increases. Modeling the F state as a rigid segment of length $d_r = 2$ nm one obtains $F^c = 15.9$ pN which is a bit farther from the experimental value.

P_r [nm]	L_r [nm]	E_y^r [pN]	ΔG^0 [$k_B T$]	N (number pair bases)
1	28.9	800	59	22

Table 2: Summary table of the parameter values used to model the RNA molecule. We use the value for the Young modulus corresponding to a ssDNA. The value for the other parameters have been taken from [10].

Another interesting magnitude to measure is the reversible work W_T^{rev} done upon the system when pulling from an initial value of $X_T = X_T^0$ up to a final value of X_T . This work is given by

$$W_T^{\text{rev}}(X_T) = G_{X_T} - G_{X_T^0} = \Delta G_{X_T} \text{ , with} \\ G_{X_T} = -k_B T \ln(Z(X_T)) = -k_B T \ln(Z_0(X_T) + Z_1(X_T)) , \quad (15)$$

where we used (8). The total reversible work in (15) defines the change in the free energy of the system. On the other hand the reversible work exerted upon the whole system is equal to the sum of reversible work exerted on each element W_h^{rev} , W_b^{rev} , W_r^{rev} (handles 1 and 2, bead and RNA molecule) by changing the total end-to-end distance from the initial to the final value of X_T :

$$W_T^{\text{rev}}(X_T) = W_b^{\text{rev}}(X_T) + W_h^{\text{rev}}(X_T) + W_r^{\text{rev}}(X_T) , \text{ where} \quad (16)$$

$$W_b^{\text{rev}}(X_T) = \langle \Delta V_b \rangle = p_0 \langle \Delta V_b \rangle_0 + p_1 \langle \Delta V_b \rangle_1 , \quad (17)$$

$$W_h^{\text{rev}}(X_T) = \langle W_h \rangle = \sum_{i=1}^2 \left[p_0 \langle W_{h_i} \rangle_0 + p_1 \langle W_{h_i} \rangle_1 \right] , \quad (18)$$

$$W_r^{\text{rev}}(X_T) = \langle W_r \rangle = p_1 (\langle W_r \rangle_1 + \Delta G^0) , \quad (19)$$

where we used (13). The functions ΔV_b , W_h and W_r correspond to the change in the potential energy of the bead in the optical trap and the work exerted upon both handles and the RNA molecule by moving the total end-to-end distance from the initial to the final value of X_T respectively. In Fig. 4 we show the different contributions to the total work W_h^{rev} , W_b^{rev} and W_r^{rev} as a function of X_T as derived from the numerical computation of $Z(X_T)$. We also show the work W_T^{rev} exerted upon the whole system. Both computations (15,16) overlap in a single curve as expected. Finally in Fig. 5 (a) we represent the TFEC for the subsystem S , $\langle f \rangle$ ¹¹ versus $\langle x \rangle$. This is obtained by numerical computation of the partition function using the relation,

$$\langle f \rangle = -\frac{\partial G_{X_T}(X_T)}{\partial X_T} = k_B T \frac{\partial \ln Z(X_T)}{\partial X_T} = k_b (X_T - \langle x \rangle) . \quad (20)$$

We also present the results obtained by averaging 1000 different trajectories in a simulation of a pulling experiment as described later in Sec. 6, and both curves show very good agreement. In Fig. 5 (b) we plot the mean force $\langle f \rangle$ as a function of the control parameter X_T .

¹¹At a given state of the system (determined by a given value of X_T) all the forces f_α are equal in average. Therefore the value of $\langle f \rangle$ referring to the mean force acting on the bead B_1 (Fig. 1) coincides with the force $\langle f_\alpha \rangle$ acting on each element α as well as on the subsystem S .

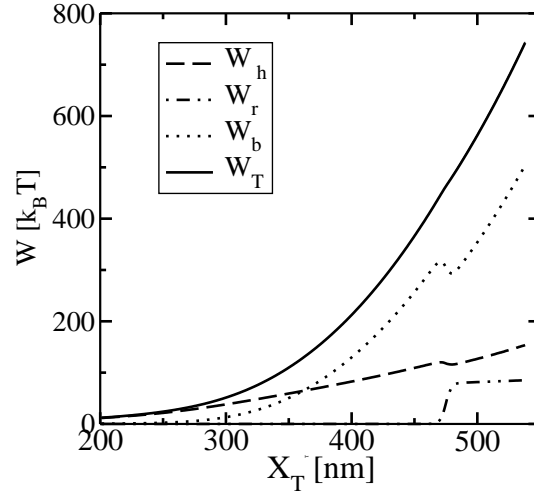


Figure 4: Different contributions to the reversible work obtained from the partition function analysis: W_T^{rev} , W_h^{rev} , W_b^{rev} and W_r^{rev} as a function of X_T . Note that the smallest contribution to the total work comes from the RNA molecule.

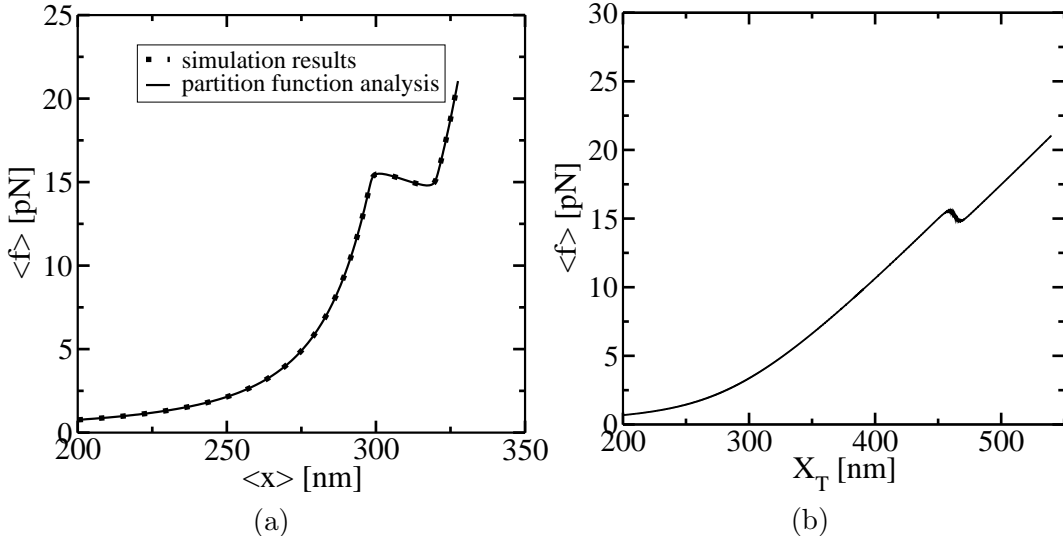


Figure 5: (a) The continuous line corresponds to the results obtained from the numerical computation of the TFEC. It is also shown the TFEC obtained by averaging over 1000 different trajectories in a simulation of a pulling experiment as explained in Sec. 6. The pulling is carried out at an approximate loading rate of 0.5pN/s (see footnote 12), slow enough to generate a quasi-static process. One can observe that both curves agree. (b) Mean force $\langle f \rangle$ as a function of the control parameter X_T . Note that there is not an abrupt vertical drop of the force at X_T^c . This is consequence of the narrow, yet observable, region of coexistence around the midpoint of the transition.

5.3 Reversible work across the transition

The quasi-static work W_{rip}^c exerted upon the subsystem S across the transition is the area under the TFEC (Fig. 6), $\langle f \rangle(\langle x \rangle)$, from $\langle x \rangle = \langle x^c \rangle_0$ to $\langle x \rangle = \langle x^c \rangle_1$, where the super-index c indicates that the system is at the midpoint of the transition where $X_T = X_T^c$ (14),

$$W_{\text{rip}}^c = \int_{\langle x^c \rangle_0}^{\langle x^c \rangle_1} dy \langle f \rangle(y) = V_b(X_T^c - \langle x^c \rangle_1) - V_b(X_T^c - \langle x^c \rangle_0) . \quad (21)$$

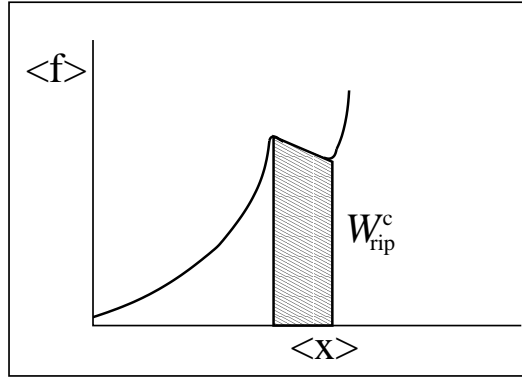


Figure 6: The shadow area under the TFEC along the transition corresponds to the quasi-static work W_{rip}^c (schematic representation).

At the midpoint of the transition both states are equally populated and (14) holds. Therefore identifying (9) and (10), we can write (21) as:

$$W_{\text{rip}}^c = \Delta G^0 + W_r^c + \Delta W_h^c, \quad (22)$$

where the functions with a super-index c are evaluated at the mean value of their variables at the critical extension X_T^c . The W_r is the loss of entropy of the RNA molecule along the transition due to the stretching and is given by (11), and the ΔW_h is the change of free energy of the handles across the transition computed as:

$$\Delta W_h = W_{h_1}(\langle x_{h_1} \rangle_1) + W_{h_2}(\langle x_{h_2} \rangle_1) - W_{h_1}(\langle x_{h_1} \rangle_0) - W_{h_2}(\langle x_{h_2} \rangle_0). \quad (23)$$

Eq. (22) tells us that the quasi-static work W_{rip}^c coincides with the change of free energy of the different elements that form the subsystem S across the transition. This W_{rip}^c is experimentally measurable as the area under the rip observed in the TFEC corresponding to the F-UF transition (Fig. 6). Therefore we can use (22) to estimate ΔG^0 from the TFEC, as explained in the next section.

5.4 Estimate of ΔG^0 from the TFEC

In Fig. 7 we show two TFECs obtained from the partition function analysis corresponding to two systems with different k_b but with the same handles and RNA molecule with parameters given in Tables 1 and 2 respectively. We use (22) in order to extract the value of ΔG^0 by computing W_{rip}^c as the area under the rip in the TFEC (Fig. 6).

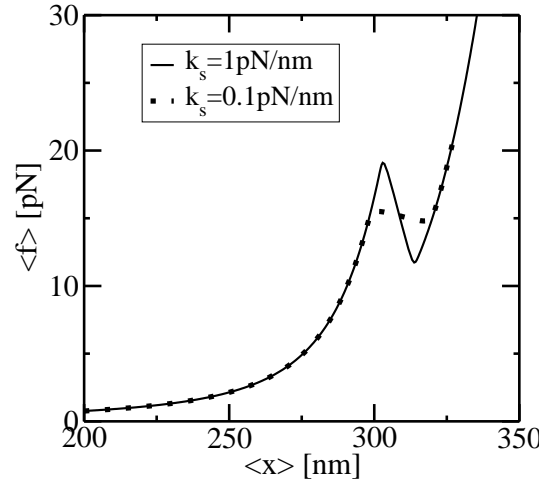


Figure 7: TFEC corresponding to two systems with handles and RNA characterized by the parameters given in Tables 1, 2 and with an optical trap stiffness $k_b = 0.1 \text{ pN/nm}$ and $k_b = 1 \text{ pN/nm}$ respectively. Note that the slope at the transition (rip) is proportional to $-k_b$.

As expected for an harmonic trap (20), the TFEC in Fig. 7 shows an slope at the transition (rip) proportional to $-k_b$. To obtain the different contributions to (22) using the WLC model [30] we first estimate $\langle x_r \rangle_1$ and $\langle x_{h_i} \rangle_1$ as the RNA and the handle i extension at the force value after the rip, $\langle f \rangle_1$, respectively. In an analogous way we estimate the $\langle x_{h_i} \rangle_0$ as the handle i extension at the force before the rip $\langle f \rangle_0$. Then we compute W_r^c and ΔW_h^c given by (11) and (23) respectively using the WLC model [30] for the TFEC $f_\alpha(x)$ for the element α with $\alpha = h_1, h_2, r$ (handles 1 and 2 and RNA respectively). Finally, we compute the area under the TFEC across the transition (rip) in order to obtain W_{rip}^c and use (22) to extract ΔG^0 . In Table 3 we show the results obtained.

k_b [pN/nm]	W_r^c [$k_B T$]	ΔW_h^c [$k_B T$]	W_{rip}^c [$k_B T$]	ΔG^0 [$k_B T$]
0.1	20	-8.5	70.5	59
1	17	-41	35	59

Table 3: Different contributions to the free energy change across the transition. As expected the value of ΔG^0 is independent of the other parameters of the system.

Note that the contribution ΔW_h^c is negative because when the RNA molecule opens the force relaxes and the handles contract, hence the free energy of the handles across the transition decreases. Neglecting the contribution that comes from the handles across the transition is a typical approximation often applied to experimental results. However we note here that this is not always possible as this contribution can be large. In the previous example, even in the case of small k_b , we would loose $8k_B T$ in the balance equation (22). The best condition to apply this approximation is to use handles characterized by a small ratio L_h/P_h as compared to the corresponding value for the RNA molecule ($L_h/P_h \ll L_r/P_r$) and a potential well with stiffness as small as possible (i.e, small k_b). In Fig. 8 we show, for a small value of k_b ($k_b = 0.1$ pN/nm), how the different contributions to (22) change when considering systems with different values for the ratio L_h/P_h . The stretching contribution to the UF state of the RNA, W_r^c , does not change when modifying the magnitude L_h/P_h , because the forces at which the transition occurs are quite stable under changes of L_h/P_h . However, the magnitude of the contribution ΔW_h^c tends to notably increase as L_h/P_h becomes larger.

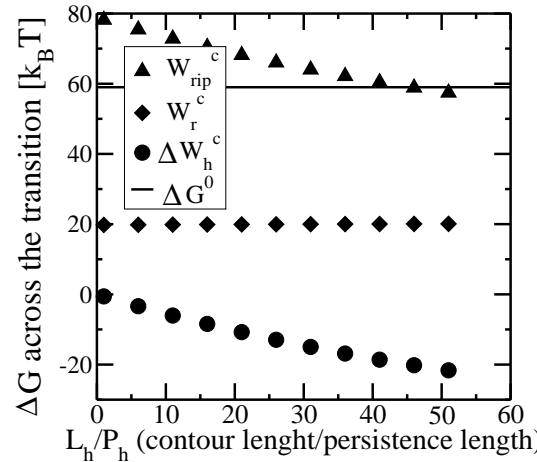


Figure 8: The different contributions to the free energy change across the transition presented as a function of the ratio L_h/P_h .

6 Simulation of a pulling experiment

As the RNA molecule unfolds-refolds in timescales much larger than the typical relaxation time of handles and bead, we can consider an instantaneous relaxation for

these latter elements to solve the dynamical equations. This hypothesis is valid as long as the data is collected at frequencies smaller than the relaxational frequency of the bead, $10^5 Hz$, that is the element with largest relaxation time (see Sec. 4). The dynamics for the RNA molecule is governed by the master equation for the probability p_σ (12),

$$\begin{aligned}\frac{dp_0}{dt} &= -k_{\rightarrow}p_0 + k_{\leftarrow}p_1 , \\ \frac{dp_1}{dt} &= -k_{\leftarrow}p_1 + k_{\rightarrow}p_0 ,\end{aligned}\quad (24)$$

where k_{\rightarrow} and k_{\leftarrow} are the unfolding and folding rates respectively. To simulate a pulling experiment we parallelly solve numerically the partition function of the system finding the mean extension and force for each element and do a numerical simulation of the dynamical model for the RNA (24). We implement the following algorithm:

- We increase X_T by $v\Delta t$, where v is the pulling speed, i.e the velocity at which the micropipette is pulled, $v = \dot{X}_T$, and Δt is the iteration time, hence $\frac{1}{\Delta t}$ is the frequency at which data is collected ¹².
- We compute the new $\langle f \rangle$ and $\langle x \rangle$ iteratively using the saddle point equations for the partition function. To these mean values we add Gaussian fluctuations of zero mean and variance given by (2). We then obtain the FEC, $f(x)$, that should qualitatively reproduce the experimental one.
- The RNA molecule is then unfolded (if it is in the folded state $\sigma = 0$) or folded (if it is in the unfolded state $\sigma = 1$) with a probability $k_{\rightarrow}(X_T)\Delta t$ and $k_{\leftarrow}(X_T)\Delta t$ respectively, where Δt is the iteration time. These probabilities come from the discretization of the master equations (24). The unfolding and folding rates, k_{\rightarrow} and k_{\leftarrow} , correspond to the rates for an activated process characterized by a barrier $B(X_T)$ and a difference of free energy between the F and UF states $\Delta G(X_T)$ (Fig. 3 (a)),

$$\begin{aligned}k_{\rightarrow}(X_T) &= k_0 \exp[-\beta B(X_T)] \\ k_{\leftarrow}(X_T) &= k_0 \exp[\beta(-B(X_T) + \Delta G(X_T))] ,\end{aligned}\quad (27)$$

where k_0 is an attempt frequency. These rates satisfy the detailed balance condition,

$$\frac{k_{\rightarrow}(X_T)}{k_{\leftarrow}(X_T)} = \exp[-\beta \Delta G(X_T)] . \quad (28)$$

The expressions of $\Delta G(X_T)$ and $B(X_T)$ are derived in appendix B using the partition function analysis.

In the simulations presented in Secs. 6.1, 6.2 we use the parameters given in Tables 1 and 2. In Table 4 we show the values of the kinetic parameters we use, such as the rate of unfolding at zero force $k_0 \exp(-\beta B^0)$ and the number of opened bases n^* that characterizes the location of the transition state (see Sec. 3)¹³.

¹² The relation between the pulling speed v and the loading rate r (velocity at which the force increases) can be found using the relation between the force and displacement increments, $\Delta f = k_{\text{eff}}(f)\Delta X_T$, as

$$r = v k_{\text{eff}} , \quad (25)$$

where k_{eff} is the effective stiffness of the system, computed as:

$$k_{\text{eff}} = \frac{d\langle f(X_T) \rangle}{dX_T} = \left[\frac{1}{k_b} + \frac{1}{k_x} \right]^{-1} , \quad (26)$$

where k_x has been defined in (3) and k_b is the stiffness of the optical trap. The F-UU transition for a small single domain of RNA typically occurs at forces in the range $8 - 20$ pN. At these forces the system verifies that k_b is much smaller than the stiffness of the handles and the RNA molecule, k_{h1}, k_{h2} and k_r , therefore we can safely assume $v = r/k_b$.

¹³ The value of n^* determines the distance from the barrier to the folded conformation, $x_1(X_T)$. With the assumption that n^* does not depend on X_T (see footnote 5) one can derive $x_1(X_T)$ using the WLC model (7) with $P = P_{RNA}$ and $L_o = L_{RNA} \frac{n^*}{N}$, $x_1(X_T) = x(f)$ where f is the mean force acting upon the system when the RNA molecule is in the transition state.

$k_0 \exp(-\beta B^0)$	n^*
$e^{-30} \approx 10^{-13}$	12

Table 4: Parameters used to characterize the kinetics of folding-unfolding of RNA. They are chosen in order to reproduce the experimental kinetics results obtained with the hairpin P5ab [10].

In what follows we present the results of our simulations performed to analyze the following aspects: i) Obtaining FECs in the mixed ensemble; ii) Computation of the fraction of forward (reverse) trajectories that have at least one refolding.

6.1 Force-extension curve results (FEC)

In Figs. 9 and 11 we show the resulting FEC of our simulations for the values used in the experiment of Liphardt et al. [10] shown in Tables 1, 2 and 4 corresponding to a P5ab RNA molecule and for a loading rate of $r = 1\text{pN/s}$ and of $r = 50\text{pN/s}$ respectively. We do the simulation for the forward and reverse processes where X_T increases and decreases in time respectively.

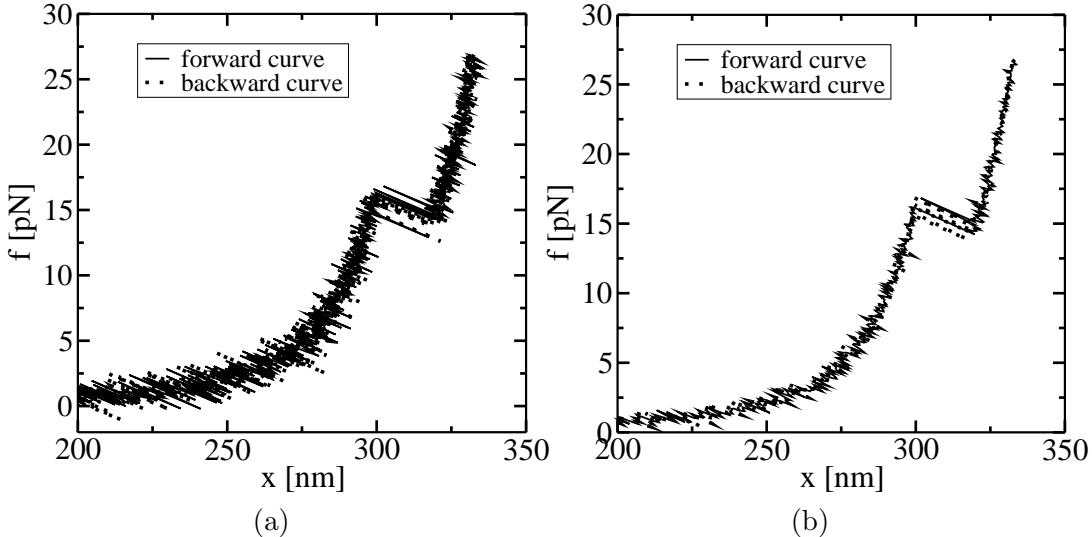


Figure 9: Results for the FEC obtained from the simulation of a pulling experiment with $r = 1\text{pN/s}$. The iteration time used in the simulation is $\Delta t = 10^{-2}\text{s}$. In (a) we show the results of calculations at each time step. In (b) we present their average over five consecutive time steps.

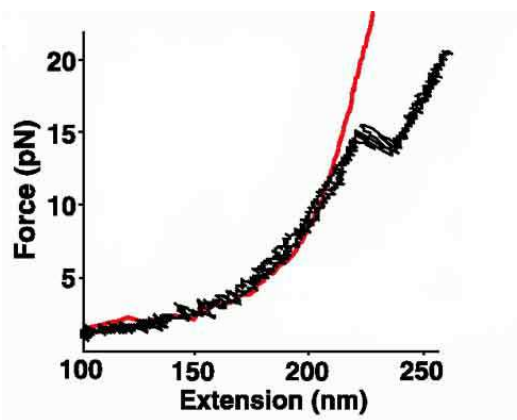


Figure 10: Experimental FEC for p5ab obtained in [10]. The continuous line corresponds to the WLC curve for the handles.

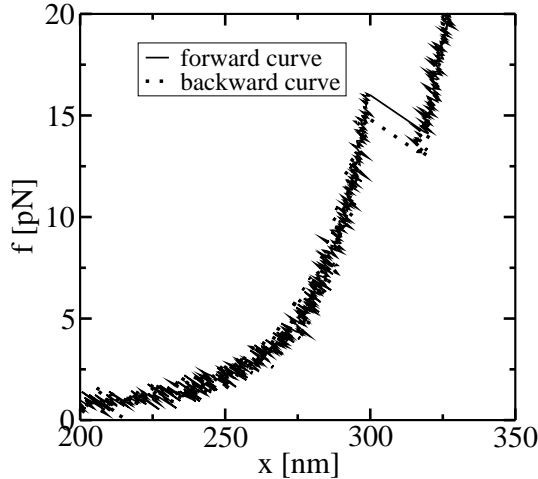


Figure 11: Results for the FEC obtained from the simulation of a pulling experiment for a $r = 50\text{pN/s}$. The iteration time used in the simulation is $\Delta t = 10^{-2}\text{s}$. At this pulling speed (v , see footnote 12) the process is not in equilibrium and hysteresis is observed around the transition.

As shown in Fig. 9, at a loading rate of 1pN/s different transition jumps are observed along both the forward and reverse processes, because the pulling speed (v , see footnote 12) is slow enough. In Fig. 9 (a) we represent the FEC resulting from the computed value of f and x at each iteration whereas in Fig. 9 (b) we show the FEC obtained after averaging the results over five consecutive iterations. The amplitude of the fluctuations observed in Fig. 9 (b) notably decreases. These values appear compatible with those found in the experimental data. Comparing these simulations results with the experimental FEC [10] shown in Fig. 10 we find a qualitative agreement, the shape of the curve around the transition region is qualitatively reproduced. However, we find some discrepancies: (i) The simulated curve is shifted in the x direction in comparison with the experimental one. This is because experimentally the quantity measured is not the absolute value of the distance x but its relative changes. Therefore in Fig. 10 the extension represented in the x -axis corresponds to changes in the value of x with respect to an initial extension of approximately 100nm . (ii) As the force increases the experimental curve separates from the theoretical WLC prediction and therefore from the simulated results. The agreement can be improved by considering bigger values for the Young modulus of the handles and of the ssRNA. Furthermore, extending the RNA molecule model to include intermediate configurations, which depend on the number of opened bases n , one realizes that the cooperative transition might not be between the F ($n = 0$) and UF ($n = N$) states, but between a partially folded and a partially unfolded states. For instance, for the P5ab RNA molecule the cooperative folding-unfolding transition is between the state $n = 3$ and the state $n = N$ [24]. This means that typically the first 3 base pairs open before the transition occurs, increasing the extension of the handles.

Fig. 11 shows the FEC corresponding to a pulling process carried out at a loading rate of $r = 50\text{pN/s}$. At this pulling speed the process is not in equilibrium and hysteresis effects are observed around the transition region.

6.2 Fraction of trajectories that have at least one refolding

We consider a system with a control parameter (generally denoted by y) that is pulled by changing y at certain speed $v(y) = \frac{dy}{dt}$. The forward (reverse) pulling process starts at a initial value of the control parameter y_i (y_f) where the RNA is in the F (UF) state and finishes at a final value of the control parameter y_f (y_i) where the RNA is in the UF (F) state. We then define N_F and N_R as the fractions of forward and reverse trajectories that have at least one refolding respectively (Fig. 12).

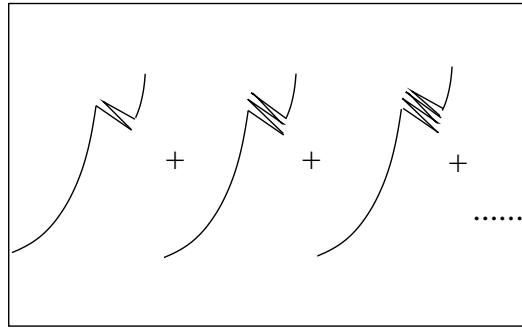


Figure 12: Different trajectories that have at least one refolding. The ratio between this sum and the total number of trajectories gives the fraction N_F (N_R) for the forward (reverse) process.

These fractions are given by

$$N_F = \int_{y_i}^{y_f} \int_y^{y_f} \frac{d\rho_0^F(y_i, y)}{dy} \frac{d\rho_1^F(y, y')}{dy'} dy' dy, \quad (29)$$

$$N_R = \int_{y_f}^{y_i} \int_y^{y_i} \frac{d\rho_1^R(y_f, y)}{dy} \frac{d\rho_0^R(y, y')}{dy'} dy' dy, \quad (30)$$

where the first integral in the right-hand side of both equations accounts for the probability of unfolding (folding) before a certain value of the control parameter y is reached and the second integral accounts for the probability of refolding once the RNA molecule has been unfolded (folded). The function $\rho_\sigma^{F(R)}(z, z')$ is the probability for the RNA molecule of remaining at state σ until $y = z'$ starting at $y = z$ in the forward (reverse) process. The ρ_σ is solution of the master equation

$$\frac{d\rho_0^{F(R)}(y, y')}{dt} = -k_{\rightarrow}(y') \rho_0^{F(R)}(y, y'); \quad (31)$$

$$\frac{d\rho_1^{F(R)}(y, y')}{dt} = -k_{\leftarrow}(y') \rho_1^{F(R)}(y, y'), \quad (32)$$

with initial condition $\rho_\sigma^{F(R)}(y, y) = 1$. In appendix C we prove that the fraction N_F is equal to N_R if the perturbation protocol for the control parameter is symmetric, i.e. if the velocities along the forward and reverse process verify $v_F(y) = -v_R(y)$. In our analysis the control parameter y corresponds to the total distance X_T and the folding-unfolding rates are given in (27). The detailed analytical expressions have been given (B-5,B-6) in the appendix B. However, working with these rates in order to do analytical computations appears quite cumbersome and it is preferable to simplify them. For analytical purposes we will consider effective rates where the functions B^1 , ΔG^1 given by (B-7) and x_1 and x_2 (the distances from the F and UF states to the transition state along the x -axis, see Fig. 3) are effective parameters independent of X_T , that we call \tilde{B} , $\tilde{\Delta G}$, \tilde{x}_1 and \tilde{x}_2 , obtaining

$$\begin{aligned} k_{\rightarrow}(f_0) &= k_0 \exp[\beta(-\tilde{B} + f_0 \tilde{x}_1 - \frac{1}{2} k_b \tilde{x}_1^2)], \\ k_{\leftarrow}(f_1) &= k_0 \exp[\beta(-\tilde{B} - f_1 \tilde{x}_2 + \tilde{\Delta G} - \frac{1}{2} k_b \tilde{x}_2^2)], \end{aligned} \quad (33)$$

where the force f_σ ($\sigma = 0, 1$) corresponds to the force acting upon the system at a given value of X_T when the RNA is in the state σ ¹⁴. In what follows we will call the dynamics generated by the effective rates (33) the effective dynamics and the ones generated by the rates (B-5,B-6) the non-effective dynamics. The effective rates are an excellent approximation to the non-effective ones in the experimental regime (see

¹⁴The approximation (33) where force does not fluctuate near the transition is well justified. In fact, when the RNA is in a given state (folded or unfolded) the magnitude of force fluctuations is negligible (the r.m.s is in the range $10^{-3} - 10^{-2}$ pN²), so one can consider the instantaneous force equal to the mean force.

appendix D). The relation between the forces f_0 and f_1 (for a fixed value of X_T) in (33) is given by

$$f_1 = f_0 - k_b \tilde{x}_m, \quad (34)$$

where \tilde{x}_m is the distance between the F and UF states, $\tilde{x}_m = \tilde{x}_1 + \tilde{x}_2$. Using (34) it is straightforward to see that the effective rates (33) satisfy the detailed balance condition (28). We can now compute the fractions (29,30) as a function of the loading rate r . In Fig. 13 we show the results obtained for the fractions N_F and N_R from the numerical computation of (29,30) using the effective dynamics (33). We also show the results obtained from the simulations for the fractions N_F and N_R as a function of the loading rate r and they agree pretty well.

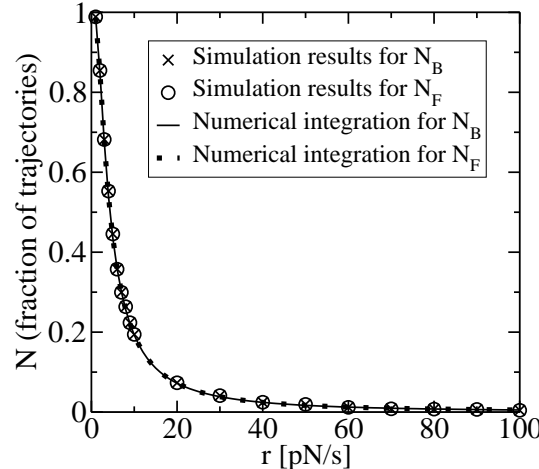


Figure 13: The fraction N_F and N_R as a function of r . It is shown the results obtained from a 5000 realizations of the simulation of a pulling experiment and also the numerical integration of (29) or (30) using the rates given by (33) characterized by the following effective parameters: $\tilde{B} \ln k_0 = 35.2 k_B T$, $\Delta G = 70.4 k_B T$, $\tilde{x}_1 = 9.75 \text{ nm}$ and $\tilde{x}_2 = 9.35 \text{ nm}$.

Through the simulation we are able to compute the mean work exerted upon the system as a function of r :

$$\langle W(r) \rangle = \left\langle \sum_{i=1}^n f_i \Delta X_T \right\rangle, \quad (35)$$

where ΔX_T is the increase in the total end-to-end distance in each iteration and n is the total number of iterations. The average is over different realizations of the simulation of the pulling process. The total work is the sum of the reversible work (i.e. the work measured in a quasi-static process for r going to zero), and the mean dissipated work that is also a function of r : $\langle W(r) \rangle = W_{\text{rev}}^T + \langle W_{\text{dis}}(r) \rangle$.

We then consider the fraction N_F for three different RNA molecules characterized by different parameters ΔG^0 , L_r , N (total number of pair bases), n^* and $B^0 \ln k_0$ and the results as a function of r are shown in Fig. 14 (a). When we plot these fractions N_F as a function of the mean dissipated work $\langle W_{\text{dis}} \rangle$ exerted upon the system we see that the three curves corresponding to the three RNA molecules collapse to a single curve as it is shown in Fig. 14 (b). This suggests that there is a generic dependence for the fraction N_F as a function of $\langle W_{\text{dis}} \rangle$. This dependence is not surprising as the average dissipated work has been already shown [18] to be a useful quantity to characterize the non-equilibrium regime. In particular, in the linear response regime, the average dissipated work depends linearly on the loading rate r , the proportionality constant being a function of the relaxation time of the molecule, the unfolding free energy and the transition force [18]. The collapse of all curves in Fig. 14 in a single curve is, however, not restricted to the linear response regime. Indeed, we have verified that in the regime $2k_B T < \langle W_{\text{dis}} \rangle < 5k_B T$, where deviations from the linear response regime are observable (Fig. 15), there is still a good collapse in Fig. 14 (b) of the curves corresponding to the three molecules. Note that by measuring the fraction N_F we

can obtain information about the value $\langle W_{\text{dis}} \rangle$, and knowing the total work we can extract the reversible work exerted upon the system. This provides an alternative way to derive equilibrium information from non-equilibrium experiments ¹⁵.

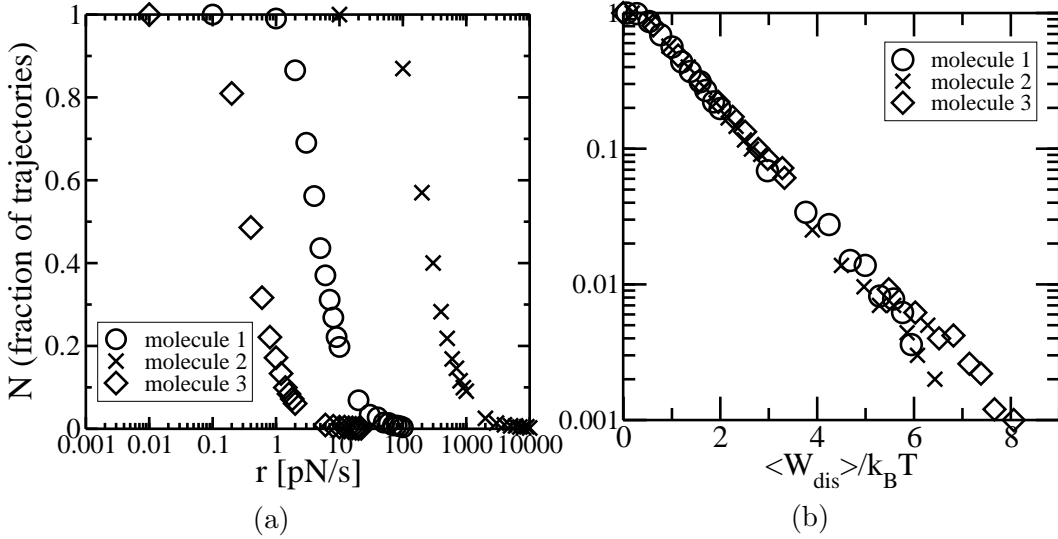


Figure 14: (a) The fraction N_F as a function of r for three different RNA molecules characterized by: Molecule (1) $\Delta G^0 = 59k_B T$, $L_r = 28.9\text{nm}$, $N = 24$, $n^* = 12$ and $B^0 \ln k_0 = 29k_B T$. Molecule (2) $\Delta G^0 = 89k_B T$, $L_r = 40\text{nm}$, $N = 34$, $n^* = 15$, $B^0 \ln k_0 = 45k_B T$. Molecule (3) $\Delta G^0 = 39k_B T$, $L_r = 16.5\text{nm}$, $N = 14$, $n^* = 9$ and $B^0 \ln k_0 = 19k_B T$. (b) The fraction N_F as a function of $\langle W_{\text{dis}} \rangle$ in logarithmic scale for the three RNA molecules considered in the left panel (a).

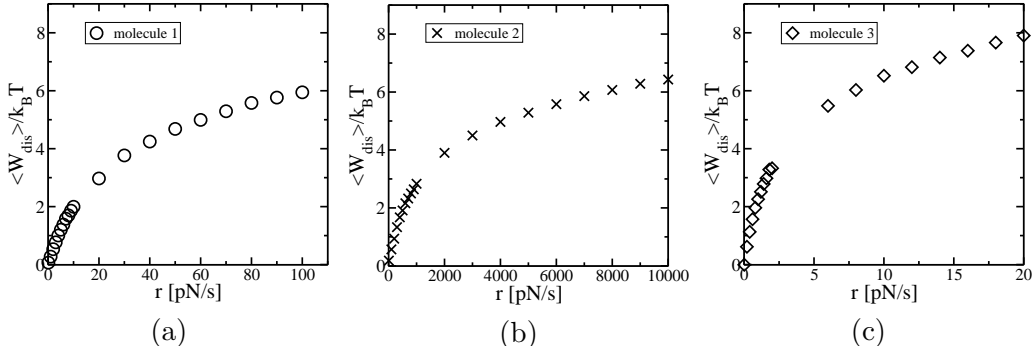


Figure 15: Mean dissipated work as a function of the loading rate r for Molecule 1 in (a), for Molecule 2 in (b) and for Molecule 3 in (c). The characteristics for the three molecules are given in Fig. 14. Note that the regimes studied are far from the linear response regime as the curves deviate from the straight lines. The deviation from the linear response regime arises at the range of r where the fraction N approaches to zero (Fig. 14 (a)).

7 Unfolding of domains stabilized by Mg^{2+} tertiary contacts

In the presence of magnesium ions (Mg^{2+}) the kinetics of the unfolding process can change dramatically if tertiary contacts are formed. In the experiments done in [10] two different RNA molecules were studied, P5ab and P5abc, with and without Mg^{2+} . The results obtained in [10] show that in presence of Mg^{2+} there are two different situations:

- If there is no formation of tertiary contacts the folding-unfolding behavior does not change qualitatively. This might be consequence of the electrostatic stabiliza-

¹⁵ Several methods has been proposed and tested [40, 41]

tion that acts homogeneously along the molecule; all base-pair hydrogen-bonds become more stable and the free energy landscape changes in a homogeneous way. This induces a slight increase of ΔG^0 and B^0 , resulting in a value of F^c that is a bit larger and a kinetics that is slower than in absence of Mg^{2+} . Indeed, this is what seems to happen in the case of the P5ab RNA molecule [10].

- When tertiary contacts stabilized by Mg^{2+} are formed the free energy landscape changes drastically, in particular in the vicinity of the bases that are involved in the formation of such tertiary contacts. Therefore the kinetics slows down dramatically and the unfolding-folding process changes totally, as observed with P5abc RNA [10].

In this Section we will focus on the study of molecules that form tertiary contacts induced by Mg^{2+} . Experiments on the unfolding kinetics of domains stabilized by Mg^{2+} tertiary contacts show how intermediate states are characterized by big barriers that are located close to the folded state along the x -axis¹⁶ [10, 11], $x_1 \ll x_m$ (Fig. 3 (a)). Consequently the height of the barrier B is quite insensitive to the force (or X_T), meaning that when the force exerted upon the system increases, B decreases much slower than the difference of free energy between both states, ΔG . Therefore big barriers and small values of x_1 imply slow unfolding processes. In complex RNA molecules the domains stabilized by the presence of Mg^{2+} -tertiary contacts are rate-limiting for the unfolding of the whole molecule [33, 34, 35, 36]. In these conditions, even at very low loading rates, the probability of refolding, once the domain is unfolded, is almost zero. The unfolding of RNA molecules with Mg^{2+} dependent barriers at experimental loading rates ($r \approx 3 - 5 \text{pN/s}$) becomes a 'stick-slip' process [11]. Therefore we can use the following transition rates¹⁷:

$$k_{\rightarrow}(X_T) = k_o e^{-B(X_T)/k_B T}, \quad k_{\leftarrow}(X_T) = 0. \quad (36)$$

These rates have been considered by Evans and Richie in the study of bond failure [12, 13]. However, in order to get a realistic modelization using the rates (36), the system requires that at the breakage force $f^*(X_T)$ (the force at which the molecule opens) the UF state is more stable than the F state, or $\Delta G(f^*(X_T)) < 0$. The breakage force changes from experiment to experiment due to the stochastic nature of the unfolding process. Therefore we expect that the distribution of breakage forces goes to zero when approaching f_m , where f_m verifies $\Delta G(f_m) = 0$, i.e. the value of the force when the RNA is in the F state at the midpoint of the transition (14), i.e $f_m = f_1(X_T^c)$. For such process, the kind of information that one can get from the analysis of the distribution of breakage forces f^* is about the kinetics rather than the thermodynamics.

In all the previous analysis we have considered the study of single domain RNA molecules. Now we want to analyze molecules that have more than one domain. In order to do that we extend the model developed in preceding sections to describe more complex RNA molecules. Here we consider how to extract kinetic information by analyzing the breakage force distribution for the case of a multidomain RNA molecule with a sequential unfolding of its domains. To this end, it is convenient to analyze first the case of a single RNA domain stabilized by Mg^{2+} tertiary contacts. As this problem has been already considered by several authors we collect some of the main results in the appendix D.

7.1 Domains with Mg^{2+} - dependent barriers that unfold sequentially under a loading rate

In this section we want to investigate the applicability of the model developed for a single domain RNA to more complex RNA molecules such as a multidomain RNA molecule with a sequential unfolding of its domains. We consider a molecule composed by different domains under the effect of an external force, focusing on the case where

¹⁶ Recent studies [32] show that the domains stabilized by Mg^{2+} tertiary contacts are better characterized by kinetic models with more than one barrier. However here we will consider the simpler case of a single barrier per domain.

¹⁷ Note that these rates do not verify the detailed balance condition.

the opening of the domains occurs in a given sequential order. There are two situations that favor a sequential unfolding of the domains. The first one relies on the topological connectivity of the molecule, that does not allow certain domains to unfold before others have not yet opened (Fig. 16 (a)). The second one is the blockade of the force induced by the most external tertiary contacts on the interior domains (Fig. 16 (b)).

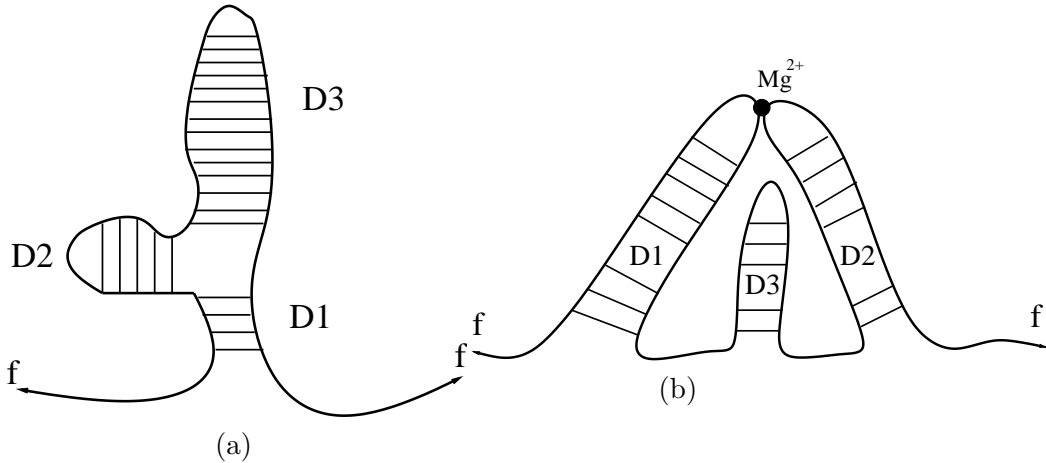


Figure 16: (a): Blockade of the force for certain domains due to the connectivity of the molecule. The force can not act over the domains D2 and D3 until D1 is not opened. (b): Blockade of the force for certain domains due to the Mg^{2+} tertiary contacts. The domain D3 does not feel the force until the Mg^{2+} tertiary contact breaks.

For sake of clarity we will consider a sequential unfolding of a multidomain RNA molecule. In general the unfolding of domains is a hierarchical process not necessarily sequential. For instance, in left panel of Fig. 16, once D1 has opened, either D2 and D3 can be unfolded. However in our modelization we unfold sequentially the domains D2 and D3. The motivation to consider this simplified model is twofold. On the one hand, there are experimental results [11] on the molecule L-21, a derivative of the *Tetrahymena thermophila* ribozyme, where the order of the opening of the different domains of the molecule studied was never observed to change. On the other hand, a main goal throughout this paper is to illustrate how the model for the experimental setup previously introduced in Secs. 2, 3, 4 can be generalized to include complex RNA molecules (and not only hairpins) rather than emphasizing details of the modeling of the RNA structure. With this proviso, we then model the RNA molecule as an unidimensional chain of single domains connected in series, each one represented as a two-states model. For a n domain system we have the F state, the UF one, and $n-1$ intermediates, I_i , where i is the index of the intermediate (Fig. 17).

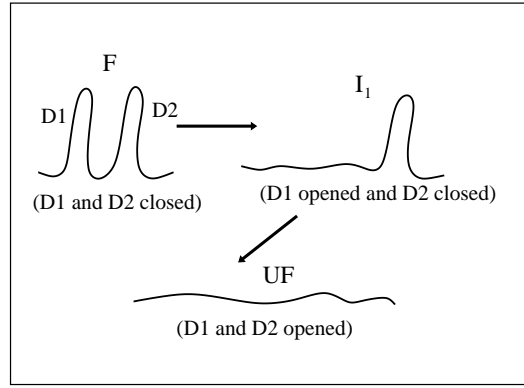


Figure 17: Representation of the different states for a 2-domain model corresponding to a molecule with two domains that sequentially unfolds. The kinetics parameters of each domain are $\tilde{x}_1^{(i)}$, $\tilde{x}_m^{(i)}$ and $\tilde{B}^{(i)}$, where the super-index $i = 1, 2$ refers to the index of the domain. The unfolding rate and the breakage force for the domain i are denoted as $k_{\rightarrow}^{(i)}$ and f_i^* respectively.

We simulate a pulling process without refolding using the effective unfolding rate given in (33) for a molecule with three domains in series. This system could represent the domain P4-P6 of the molecule L-21, recently investigated [11]. In these experiments, it is observed a sequential unfolding of the domains, even though there are different unfolding pathways because not all the intermediates are seen in each trajectory (sometimes two consecutive domains open simultaneously). The most frequently observed pathway contains three transitions corresponding to the consecutive opening of the domains P4P6, P5 and P5abc. In Fig. 18 we show the FEC of a 3-domain RNA system and in Fig. 19 the histograms for the starting position of the rips detected. The results shown in Figs. 18 (a) 19 (a) have been obtained by doing a numerical simulation of a pulling experiment using the parameters for the handles and the bead given in Table 1. The kinetic parameters of each RNA domain are given in Fig. 18. In panels (b) of these figures are shown the experimental results [11].

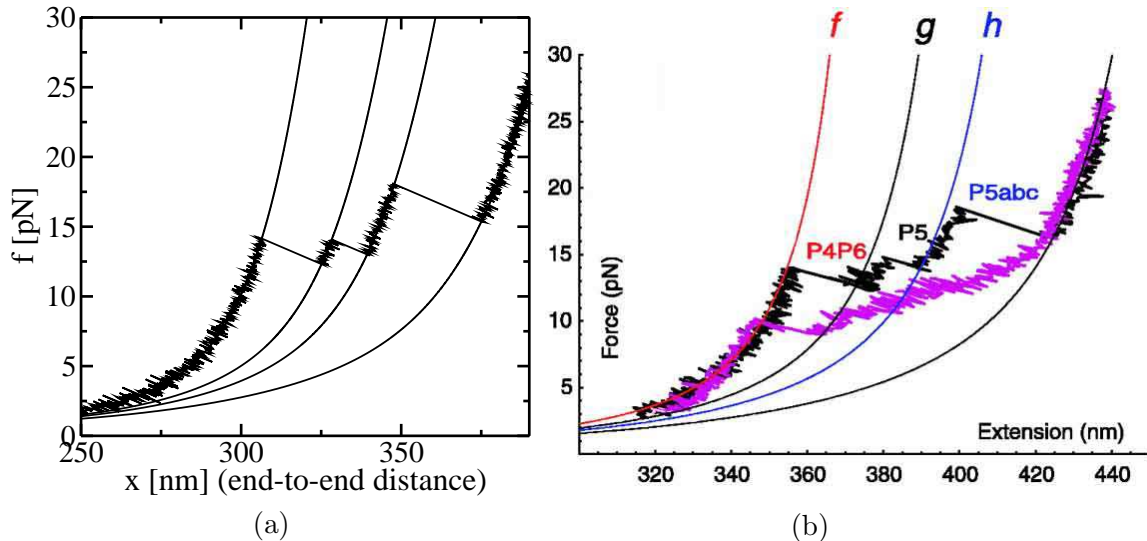


Figure 18: Comparison of FECs between model and experiments. (a) Numerical simulations of the pulling process are at $r = 4\text{pN/s}$ for three RNA domains. Simulations have been done with the effective model (33) without refolding. Domains characterized by $\tilde{x}_1^{(1)} = 2.5\text{nm}$ $\tilde{B}^{(1)} \ln(k_o^{(1)}) = 8.5k_B T$, $\tilde{x}_1^{(2)} = 2.5\text{nm}$ $\tilde{B}^{(2)} \ln(k_o^{(2)}) = 8k_B T$, $\tilde{x}_1^{(3)} = 1.7\text{nm}$ $\tilde{B}^{(3)} \ln(k_o^{(3)}) = 8.5k_B T$, where the super-index refers to the index of the domain. The solid lines correspond to the WLC force-extension curves. (b) Experimental FEC for the P4-P6 domain obtained in [11]. The solid lines correspond to WLC curves for the handles linked to the RNA molecule. The lower curve correspond to the refolding process that we do not consider here. Figure taken from [11].

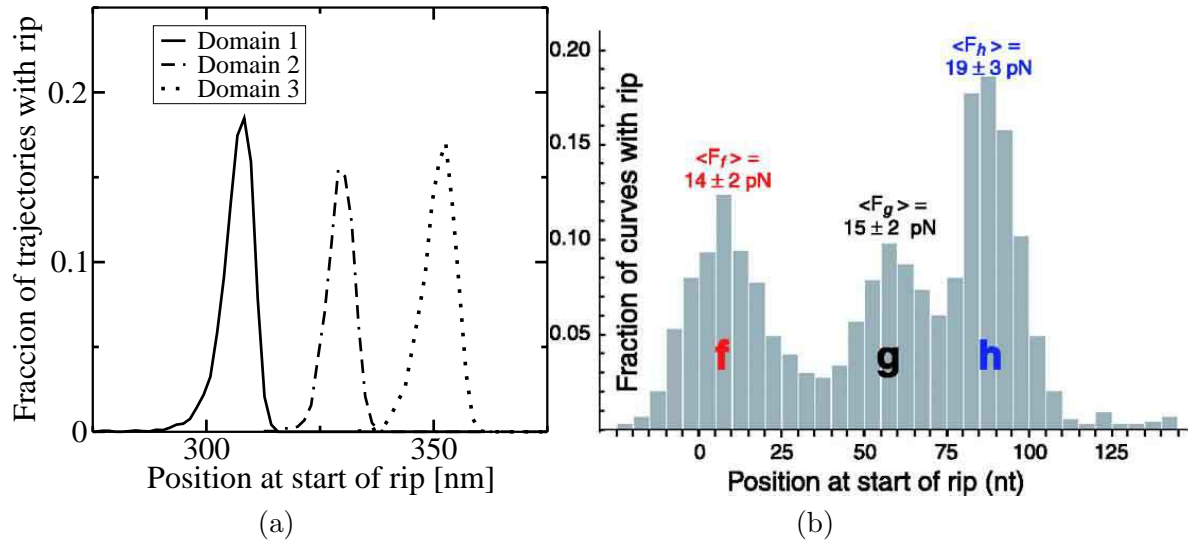


Figure 19: Comparison between model and experiments of the rip position distribution. (a) Histograms for the positions at the start of the detected rips. They correspond to the three transitions observed in Fig. 18 (a). The parameters used in the simulation are given in Fig. 18 (a). (b) Experimental histograms of rips detected in 732 unfolding curves of P4-P6 (Fig. 18 (b)). Figure taken from [11].

For the third domain, that corresponds to the well known domain P5abc, we use the values of the parameters $\tilde{x}_1^{(3)}$ and $\tilde{B}^{(3)} \ln(k_o^{(3)})$ obtained in [10]. We choose the parameters for the other domains in order to qualitatively reproduce the experimental results for the unfolding trajectories in [11] shown in the right panel of Fig. 18. The histograms for the positions at the start of the rips detected obtained from these values of parameters are different from the experimental ones (Fig. 19). The main difference comes from the amplitude of the fluctuations of the position where each domain opens, that is smaller in simulations results as compared to experimental results ¹⁸. Several reasons can explain this disagreement. First, there are strong drift effects in the machine that introduce instrumental noise. Second, no two pulled molecules are ever identical (disparity of the attachments, existence of more than one tether on the beads that can influence force measurements). A dispersion in the population of molecules is always another source of noise. Third, the RNA molecule is not just composed by a series of domains, but there are other regions (some bases) that do not belong to any domain. These regions can contribute differently to increase the length of the rips, a source of randomness for the position of the start of the rips. Last but not least, we cannot exclude that the kinetic model we are considering is too simple to explain the unfolding of these domains. It is known that complex RNA structures show characteristic FECs that cannot be usually interpreted in terms of the successive opening of native domains, because of the existence of long-lived intermediates including non-native helices [39].

The most important difference between the analysis of a single barrier (see Appendix D) and the present study of a succession of n domains is that the force does not reach the domain i until the previous domain $i-1$ has opened. Then the domain i starts to be pulled only at a force larger than f_i^s , which in our approximation is given by:

$$f_i^s = f_{i-1}^* - k_b \tilde{x}_m^{(i-1)} . \quad (37)$$

where the parameters and functions with index i refer to the domain i . Let us define the quantity C_i as:

$$C_i = \frac{k_B T}{r \tilde{x}_1^{(i)}} k_{\rightarrow}^{(i)}(f_i^s) . \quad (38)$$

¹⁸Note that in experimental results the distances are given in units of nucleotides but our results are in units of nanometers. In the totally extended form of the polymer the conversion unit is 0.59 nm per nucleotide.

The average value over different trajectories of this quantity $\langle C_i \rangle$ is a measure of the probability of opening the domain i just after the domain $i-1$ has been opened. According to the value of $\langle C_i \rangle$ we can distinguish three different regimes:

1. $\langle C_i \rangle \ll 1$. Most of trajectories show two separated transitions (rips) for the opening of the domain $i-1$ and i , because at the typical value of f_i^s there is a low probability of opening the domain i . It is then possible to treat the domain i independently of the $i-1$, as a single domain, using (D-1) to analyze the distribution of breakage forces.
2. $\langle C_i \rangle \gg 1$. The probability of opening the domain i at f_i^s is large. Therefore most of the time one observes a single transition (rip) for the opening of both domains and the intermediate state I_{i-1} is hardly observable. In this case it is not possible to obtain information about the domain i .
3. $\langle C_i \rangle \approx 1$. This is the intermediate case between the two previous ones. We expect to observe trajectories with a single transition (1 rip) for the opening of the domains i and $i-1$ and other ones with two separated transitions (2 rips). In this case, to obtain kinetic information of domain i from the analysis of the distribution of breakage force, f_i^* , we need to recalculate the distribution of the breakage force as shown in appendix E or to work with the distribution of f_i^* conditioned to the fact the domain $i-1$ has been opened at a force smaller than a given value.

We focus on the study of the regime 3 considering two different two-domain molecules coupled to the system described in Sec. 2 with parameters given in Table 1. The system is pulled at $r = 4\text{pN/s}$. The first domain is the same for both molecules and its kinetics parameters are $\tilde{x}_1^{(1)} = 2.5\text{nm}$ and $\tilde{B}^{(1)} \ln(k_o^{(1)}) = 8.5k_B T$; the second domain is different for the two molecules, but both have $\langle C_2 \rangle$ of order of 1, so they are in regime 3. In order to get the kinetics parameters for the second domain, we will use two different techniques:

- In appendix E we compute the distribution of breakage forces for a domain i in regime 3 (E-4), as a function of the kinetics parameters of domain i and the previous one $i-1$. This technique uses the expression (E-4) to extract kinetic information for the second domain from the kinetics parameters of the first domain. The method consist in first building an histogram of the breakage forces for the second domain, using the results from all the trajectories¹⁹. Then we fit the histogram to the distribution (E-4)²⁰ to get the kinetics parameters for the second domain. The results obtained are shown in Fig. 20.

¹⁹For the trajectories where only a single transition is observed for the opening of the first and second domains, it is possible to compute the breakage force for the second domain f_2^* as: $f_2^* = f_1^* - k_b \tilde{x}_m^{(1)}$.

²⁰We truncate the series at certain k once we find convergence.

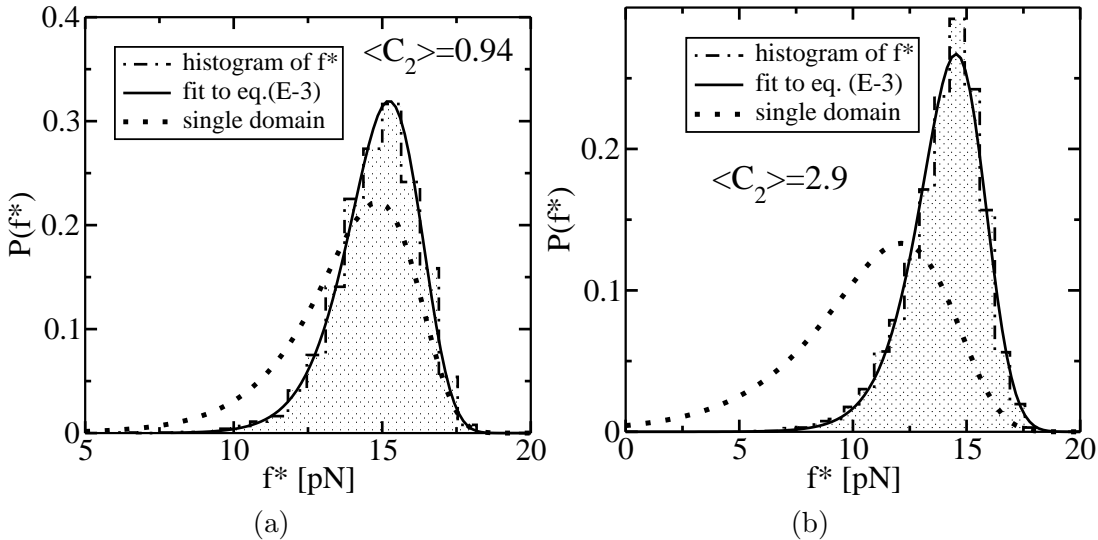


Figure 20: Histogram of breakage forces for the second domain of a two domain system characterized by given values of $\tilde{x}_1^{(2)}$, $\tilde{B}^{(2)} \ln(k_o^{(2)})$. The continuous line is the best fit to (E-4), truncating the series at a value $k = k^*$ where convergence is achieved. The dotted line shows the distribution of breakages forces for a single domain for the real values of $\tilde{x}_1^{(2)}$ and $\tilde{B}^{(2)} \ln(k_o^{(2)})$. (a): System with $\tilde{x}_1^{(2)} = 2.5\text{nm}$ and $\tilde{B}^{(2)} \ln(k_o^{(2)}) = 8k_B T$. Series summation was truncated at $k^* = 2$. The fit gives $\tilde{x}_1^{(2)} = 2.6 \pm 0.1\text{nm}$ and $\tilde{B}^{(2)} \ln(k_o^{(2)}) = 8.2 \pm 0.3k_B T$ in agreement with the correct values. The average value for the parameter C_i for this domain is $\langle C_2 \rangle = 0.94$. These are results obtained from 1000 pulls. (b): System with $\tilde{x}_1^{(2)} = 1.5\text{nm}$ and $\tilde{B}^{(2)} \ln(k_o^{(2)}) = 4k_B T$. Series summation was truncated at $k^* = 3$. The fit gives $\tilde{x}_1^{(2)} = 1.6 \pm 0.1\text{nm}$ and $\tilde{B}^{(2)} \ln(k_o^{(2)}) = 4.3 \pm 0.3k_B T$ in agreement with the correct values. The average value for the parameter C_i for this domain is $\langle C_2 \rangle = 2.9$. These are results obtained from 1000 pulls.

- The second technique consist on working with the probability distribution that the domain i opens at a force f_i^* conditioned to the fact that the previous domain opened at a force f_{i-1}^* smaller than a given force f_l , $\rho(f_i^* | f_{i-1}^* < f_l)$. Considering small values of f_l , the distribution $\rho(f_i^* | f_{i-1}^* < f_l)$ gets closer to the distribution of a single domain (D-1). For instance if we consider $f_l < \tilde{f}$, where \tilde{f} is the minimal force at which there is no probability of unfolding the domain i at the given r ²¹, the conditioned distribution overlaps with the distribution for a single domain. To compute $\rho(f_i^* | f_{i-1}^* < f_l)$, we do histograms of breakage forces for the set of trajectories that verify $f_{i-1}^* < f_l$. Starting with a certain value of f_l we build the histogram and do the fit to (D-1) to get the kinetics parameters, $\tilde{x}_1^{(i)}$ and $\tilde{B}^{(i)} \ln(k_o^{(i)})$. Then we repeat the process decreasing the value of f_l until the parameters obtained from the fit converge to a given value; in this regime of values of f_l the domain i is not influenced by the previous domain, and one gets the right values for the kinetics parameters. The drawback of this technique is that for f_l too small the number of useful trajectories quickly decreases, and one needs many more pulls to be able to build an histogram. In the following figure 21 we show our results for $\rho(f_2^* | f_1^* < f_l)$, for the two molecules considered before.

²¹The force \tilde{f} represents the lower limit force value below which the distribution of breakage force goes to zero.

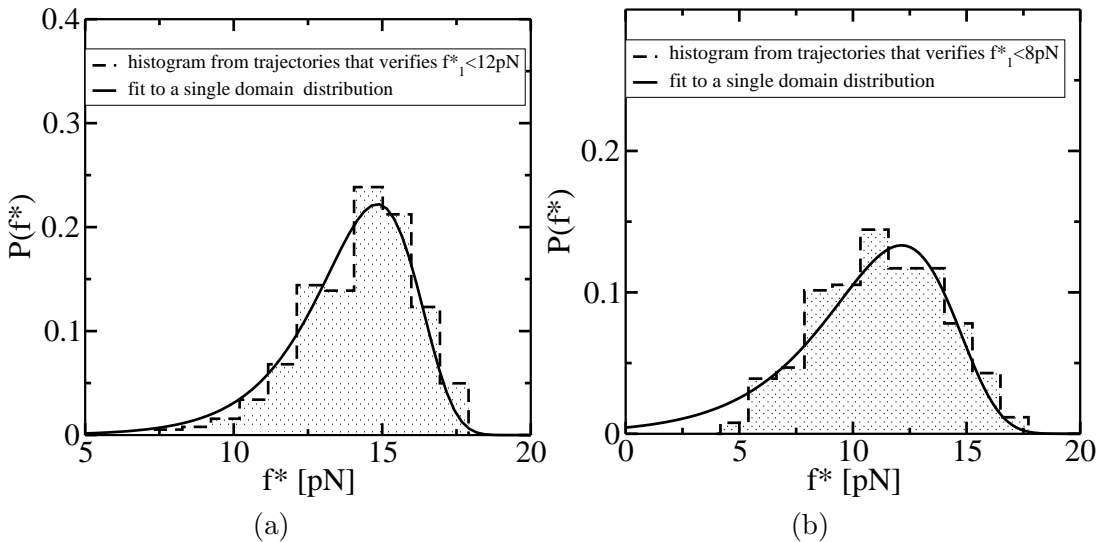


Figure 21: Histogram of breakage forces for the second barrier of a two domain RNA molecule for the set of trajectories that verify $f_1^* < f_l$ (the first domain opens at a force smaller than f_l). The continuous line corresponds to the distribution of breakages forces for a single domain for the real values of $\tilde{x}_1^{(2)}$ and $\tilde{B}^{(2)} \ln(k_o^{(2)})$. (a): Same parameters as in Fig. 20 (a). System characterized by $\tilde{x}_1^{(2)} = 2.5\text{nm}$ $\tilde{B}^{(2)} \ln(k_o^{(2)}) = 8k_BT$, $f_l = 12\text{pN}$. The fit to (D-1) gives $\tilde{x}_1^{(2)} = 2.5 \pm 0.1\text{nm}$ and $\tilde{B}^{(2)} \ln(k_o^{(2)}) = 8.0 \pm 0.4k_BT$. Histograms were obtained from 3000 pulls and 392 pulls verify $f_1^* < 12\text{pN}$. (b): Same parameters as in Fig. 20 (b). System characterized by $\tilde{x}_1^{(2)} = 1.5\text{nm}$, $\tilde{B}^{(2)} \ln(k_o^{(2)}) = 4k_BT$, $f_l = 8\text{pN}$. The fit to (D-1) gives $\tilde{x}_1^{(2)} = 1.5 \pm 0.1\text{nm}$ and $\tilde{B}^{(2)} \ln(k_o^{(2)}) = 3.7 \pm 0.3k_BT$. Histograms were obtained from 15000 pulls and 204 pulls verify $f_1^* < 8\text{pN}$.

We conclude that in order to obtain kinetic information for a domain in regime 3 both techniques are complementary. The first technique has the disadvantage that it requires the knowledge of the kinetic parameters of the previous domain. The method to extract information about the second domain is to start with the analysis of the first domain (that is not blocked by any domain) and going forward following the sequential order in which domains open. On the other hand, the problem of the second technique is that when considering small values of f_l the number of useful trajectories quickly decreases, and one needs a large number of pulls to be able to build an histogram. Depending on the experimental conditions one can decide which technique is the best to apply.

8 Conclusions

The recent fast development of nanotechnologies allow scientists to investigate the physical behavior of complex biomolecules. Of particular importance are those physical processes in the nanoscale where the typical values of the energies involved are several times k_BT . In such regime fluctuations and large deviations from the average behavior are important and deserve a careful investigation as they can contribute a lot to the understanding of thermal processes in small systems. RNA pulling experiments offer an excellent framework to address such questions as RNA molecules can be small enough for stochastic fluctuations be observable and measurable.

An extremely useful technique to manipulate individual molecules are optical tweezers which cover a range of forces 1-100 pN that is relevant for many biological processes. A full understanding about how to extract accurate physical information from such experiments is therefore of great importance. The present work represents an attempt in that direction. At present it is not yet possible to unfold individual RNA molecules without attaching some polymer handles at their extremes, therefore all RNA pulling experiments are carried out with a system larger than the individual “naked” RNA molecule. This system includes the RNA molecule, the polymer handles and the bead in the optical trap. In order to extract accurate physical information

regarding the RNA molecule, a global treatment of the whole system is necessary.

In this paper we analyzed the minimal system required to interpret the data extracted from RNA pulling experiments. We did not include any details regarding the response of the machine or a realistic and accurate modelization of the structure of the RNA molecule. On the contrary, we have focused on those thermodynamic and kinetic aspects of pulling experiments by considering the transmission of the force on the RNA molecule induced by the bead and handles. A key part of our treatment is a proper consideration of the ensemble that is relevant in pulling experiments. While the end-to-end distance (between the bead and the micropipette) and the force are variables that fluctuate, the total end-to-end distance X_T (Fig. 1) does not. The thermodynamic potential in such ensemble is the key quantity that allows us to extract accurate knowledge of the influence of these external parts (beads and handles) on the thermodynamic and kinetic behavior of the RNA molecule.

In Sec. 3 we introduce the appropriate thermodynamic potential by focusing the analysis on single domain RNA molecules that show a highly cooperative folding-unfolding behavior. In Sec. 5 we analyzed the thermodynamics of the whole system by doing a partition function analysis that includes all parts of the setup previously described in Sec. 4. Four are the most important results in Sec. 5: a) we get an explicit expression (14) for the transition force F^c as well as we are able to reconstruct the thermodynamic force-extension curve (TFEC) from the knowledge of the parameters of the model, see (20); b) The different contributions to the total reversible work (16), coming out from the different parts of the system (bead, handles and RNA molecule), have been analyzed (17,18,19). A comprehensive summary of these results is shown in Fig. 4; c) A relation between the unfolding free-energy of the molecule ΔG_0 and the area under the force rip W_{rip}^c has been given in (22). d) Finally the dependences of the free-energy contributions to the total reversible work across the transition were analyzed as a function of the stiffness of the trap and the ratio between the contour and persistence lengths of the polymer handles (Fig. 8 and Table 3). Taken together all these results establish a framework to infer thermodynamic properties of the RNA molecule from the experimental data. Moreover, they also allow us to understand under which conditions (parameters for the bead and handles) it is more reliable to get estimates for these properties.

From the thermodynamics to the kinetics we verify in Sec. 6 that the model studied qualitatively reproduces the results reported from experiments (Figs. 9 and 10) doing a numerical simulation of a pulling experiment. In Sec. 6.2 we obtain some interesting results for other quantities that are amenable to experimental checks. In particular, we find a generic relation between the fraction of molecules that unfold (refold) at least twice during the unfolding (refolding) and the mean dissipated work. Interestingly this relation is valid beyond the linear response regime where the dissipated work does not increase linearly with the pulling speed. This relation could allow us to extract the reversible work for the unfolding process by using data extracted from non-equilibrium pulling experiments. This procedure is reminiscent of other techniques, recently applied to RNA pulling experiments [40], based on the Jarzynski equality or similar relations (for a recent review, see [41]). Moreover we have shown a symmetry property that relates these fractions for the forward and reverse processes. How general this result is in general transition state theory [42] (i.e. beyond the case of a cooperative two-states system) remains an interesting open question.

In order to stress the adaptability and feasibility of our model to describe more complex type of molecules we consider in Sec. 7 the unfolding of a large RNA molecule made out of different domains that unfold sequentially. The unfolding of these domains is controlled by Mg^{2+} tertiary interactions which induce large energy barriers, thereby a refolding event (while the molecule is pulled) is not observed at experimental conditions. Although our study is not complete for such type of molecules (the assumption of a sequential unfolding may not consider other possible unfolding pathways) it is instructive to see that by modifying only the model for the RNA molecule we are still capable of qualitatively reproducing several experimental results as shown in Figs. 18 and 19. Finally we discuss possible ways to extract information about the kinetics of a single domain from the analysis of the breakage force distribution in a regime where the distribution of the breakage force for a domain depends on the

presence of a previous domain.

Many aspects of RNA pulling experiments are still open, among them would be interesting to extend these considerations to include more complex effects induced by the response of the machine, test experimentally some of the results predicted in this work for the fraction of unfolded events and also a detailed investigation of the kinetics of the folding process (rather than the unfolding) in the presence of force, a process for which we still lack an understanding. Several of these aspects will be addressed in the near future.

Acknowledgments

We thank C. Bustamante, J. Liphardt, I. Tinoco and S. Smith for insightful discussions. We also thank I. Pagonabarraga and G. Franzese for discussions as well as a critical reading of the manuscript. M. Mañosas has been supported by U.B Grant and F. Ritort has been supported by the David and Lucile Packard Foundation, the European community (STIPCO network), the Spanish research council (Grant BFM2001-3525) and the Catalan government.

A Partition function in mixed ensemble

The partition function, $Z(X_T)$, for the system described in Fig. 1, gives the free energy G_{X_T} as well as other relevant thermodynamic properties. The state of the system is defined by the externally controlled variables X_T , T and P . The last two, T and P , are always kept at a constant value so we can ignore them throughout the paper. The partition function for this one-dimensional system can be written as the convolution of the contributions coming out from the different elements ²²:

$$Z(X_T) = C \int_0^{L_1} dx_{h_1} \int_0^{L_2} dx_{h_2} \int_0^{\infty} dx_b \int_0^{L_r} dx_r \left[Z^{h_1}(x_{h_1}) Z^{h_2}(x_{h_2}) Z^s(x_b) Z^r(x_r) \times \delta(X_T - (x_{h_1} + x_{h_2} + x_b + x_r)) \right], \quad (\text{A-1})$$

where $Z^\alpha(x_\alpha)$ is the partition function distribution of the element α , with $\alpha = h_1, h_2, r, b$. The lengths L_1 , L_2 and L_r are the contour lengths of the handles 1, 2 and the single stranded RNA (ssRNA) respectively. The constant C is a normalization factor. The distribution $Z^\alpha(x_\alpha)$ for the element α is computed as:

$$Z^\alpha(x_\alpha) = g_\alpha(x_\alpha) e^{-\beta E_\alpha(x_\alpha)} = e^{-\beta G_\alpha(x_\alpha)}, \quad (\text{A-2})$$

with $\beta = \frac{1}{k_B T}$. The functions $E_\alpha(x_\alpha)$ and $G_\alpha(x_\alpha)$ are the energy (or enthalpy) and the Gibbs free energy of the element α respectively. Both are related by $G_\alpha(x_\alpha) = E_\alpha(x_\alpha) - TS_\alpha(x_\alpha)$ where $S_\alpha(x_\alpha)$ is the entropy, $S_\alpha(x_\alpha) = k_B \ln(g_\alpha(x_\alpha))$ and $g_\alpha(x_\alpha)$ is the density of states. We now compute the free energy G_α , of each of the different elements at fixed value of x_α :

- Bead trapped in a potential well: As the $V_b(x)$ is the potential of mean-force for the bead in the trap along the reaction coordinate (see footnote 2) we can write,

$$Z^s(x_b) = e^{-\beta V_b(x_b)}. \quad (\text{A-3})$$

- Handles: We use the fact that the difference of free energy between the state defined with $x = 0$ and the one with $x = x_{h_i}$ is equal to the reversible work performed by stretching the handle from $x = 0$ to $x = x_{h_i}$,

$$G_{h_i}(x_{h_i}) = \int_0^{x_{h_i}} dx f_{h_i}(x) = W_{h_i}(x_{h_i}), \quad \text{for } i = 1, 2 \quad (\text{A-4})$$

²²We restrict the configurational space to positive values of the variables x_α , with $\alpha = h_1, h_2, r, b$. The reason of taking this simplification is because when considering positive values of the control parameter X_T the configurations with negative values of some x_α have practically no weight.

where $f_{h_i}(x)$ is the thermodynamic force-extension curve (TFEC) of the handle i ²³. We get

$$Z^{h_i}(x_{h_i}) = e^{-\beta W_{h_i}(x_{h_i})} . \quad (\text{A-5})$$

- RNA: The partition function Z^r can be divided in two parts, one corresponding to the F state ($\sigma = 0$) and the other to the UF state ($\sigma = 1$). In the present analysis we are considering that the F state is represented by a single configuration while the UF states are represented by a continuous set of configurations corresponding to the difference extensions of the ssRNA (Fig. 3 (b)). Therefore Z^r is made up of two terms: a singular contribution that comes from the F state ($\sigma = 0$) represented by a delta function and a continuous contribution that comes from the UF state ($\sigma = 1$). We take the F state as the reference state with zero free energy. The free energy of the UF state has two terms: the free energy at zero force, ΔG^0 , plus the corresponding loss of entropy due to the stretching:

$$Z^r(x_r) = Z(x_r, \sigma = 0) + Z(x_r, \sigma = 1) = \delta(x_r) + C_r e^{-\beta(\Delta G^0 + W_r(x_r))} , \quad (\text{A-6})$$

where $W_r(x_r)$ is computed as in (A-4)

$$W_r(x_r) = \int_0^{x_r} dx f_r(x) , \quad (\text{A-7})$$

being $f_r(x)$ the TFEC of the ssRNA polymer. The probability $P(\sigma)$ for the RNA molecule to be in the state σ is given by $P(\sigma) \propto \int_0^{L_r} dx_r Z(x_r, \sigma)$. To compute C_r we use that the RNA molecule at zero force satisfies

$$\Delta G^0 = -k_B T \ln\left(\frac{P(\sigma = 1)}{P(\sigma = 0)}\right) \quad (\text{A-8})$$

and substituting (A-6) we obtain,

$$C_r = \frac{1}{\int_0^{L_r} dx e^{-\beta W_r(x)}} . \quad (\text{A-9})$$

Adding the different contributions we get:

$$\begin{aligned} Z(X_T) &= C \int_0^{L_1} dx_{h_1} \int_0^{L_2} dx_{h_2} \int_0^{\infty} dx_b \int_0^{L_r} dx_r \left[e^{-\beta(W_{h_1} + W_{h_2} + V_b)} \right. \\ &\times \left. [\delta(x_r) + C_r e^{-\beta(\Delta G^0 + W_r)}] \delta(X_T - (x_{h_1} + x_{h_2} + x_b + x_r)) \right] . \end{aligned} \quad (\text{A-10})$$

We now separate (A-10) in two contributions coming from the F and the UF states. By using the integral representation of the delta function,

$$\delta(x) = \frac{1}{2\pi} \int_{-\infty}^{\infty} \exp(i\lambda x) d\lambda \quad (\text{A-11})$$

we get

$$Z(X_T) = Z_0(X_T) + Z_1(X_T) \text{ with} \quad (\text{A-12})$$

$$Z_0(X_T) = \frac{C}{2\pi} \int_{-\infty}^{\infty} d\lambda e^{(i\lambda X_T + g_0(\lambda))} \text{ and } Z_1(X_T) = \frac{C}{2\pi} \int_{-\infty}^{\infty} d\lambda e^{(i\lambda X_T + g_1(\lambda))} , \quad (\text{A-13})$$

²³ Which variables are controlled is a relevant choice in single molecule pulling experiments. In contrast with macroscopic systems, where all the ensembles are equivalent [15], FECs depend on the particular ensemble considered. Eq. (A-4) has been defined for the isometric ensemble. The isometric TFEC is the thermodynamic curve corresponding to a system in the ensemble where the end-to-end distance x is held fixed, and is given by the mean force as a function of x , $\langle f \rangle(x)$. While the isotensional TFEC is the TFEC resulting of working in the force ensemble, $\langle x \rangle(f)$. In general both TFEC differ [15], but in this analysis we consider that the handles and the RNA molecule are long and flexible enough to have an identical isometric and isotensional TFEC that we call $f_\alpha(x_\alpha)$ with $\alpha = h_1, h_2, r$. This allow us to use the extrapolation expression (7) (or the one given in [30]) for the function $f_\alpha(x_\alpha)$ when using the WLC model to describe the polymer behavior.

where the functions g_0 and g_1 are given by

$$g_0 = \log \left[\int_0^{L_1} dx_{h_1} \int_0^{L_2} dx_{h_2} \int_0^{\infty} dx_b [e^{-\beta(W_{h_1} + W_{h_2} + V_b)} e^{-i\lambda(x_{h_1} + x_{h_2} + x_b)}] \right], \quad (\text{A-14})$$

$$g_1 = \log \left[\int_0^{L_1} dx_{h_1} \int_0^{L_2} dx_{h_2} \int_0^{\infty} dx_b \int_0^{L_r} dx_r [C_r e^{-\beta(W_{h_1} + W_{h_2} + V_b + \Delta G^0 + W_r)} e^{-i\lambda(x_{h_1} + x_{h_2} + x_b + x_r)}] \right]. \quad (\text{A-15})$$

Eqs. (A-13) for Z_0 and Z_1 are integrals respect to λ of an exponential with an argument that is extensive with the size of the system²⁴. Therefore if the system is big enough, the saddle point approximation is valid and becomes exact in the thermodynamic limit. As a check we have verified that the results from the saddle point approximation and the exact numerical integration of the partition function are in pretty good agreement for the system with parameters given in Tables 1 and 2. Applying the saddle point technique, one is led to extremize the arguments of the exponentials with respect to all the variables of integration. In this way we obtain:

$$\frac{dg_\sigma}{dx_\alpha} \Big|_{x_\alpha=\tilde{x}_\alpha^\sigma} = \tilde{\lambda}_\sigma \quad \text{with } \sigma = 0, 1 \quad \text{and } \alpha = h_1, h_2, r, b, \quad (\text{A-16})$$

where \tilde{x}_α^σ corresponds to the value of the variable x_α when the RNA molecule is in the state σ that extremizes the argument of the exponential. We have two branches corresponding to the situations where the RNA is folded ($\sigma = 0$) and where the RNA is unfolded ($\sigma = 1$). We use the super-index σ to denote each branch. Eq. (A-16) tells that the integration variable λ plays the role of the thermodynamic force, so the $\tilde{\lambda}_\sigma$ corresponds to the mean force acting upon the system for the branch σ and for a fixed value of X_T called $\langle f \rangle_\sigma$. Eq. (A-16) can be written as

$$\begin{aligned} f_b^0(\tilde{x}_b^0) &= f_{h_1}^0(\tilde{x}_{h_1}^0) = f_{h_2}^0(\tilde{x}_{h_2}^0) = \langle f \rangle_0, \\ f_b^1(\tilde{x}_b^1) &= f_{h_1}^1(\tilde{x}_{h_1}^1) = f_{h_2}^1(\tilde{x}_{h_2}^1) = f_r^1(\tilde{x}_r^1) = \langle f \rangle_1, \end{aligned} \quad (\text{A-17})$$

where the force $f_\alpha^\sigma = \langle \frac{dW_\alpha^\sigma(x)}{dx} \rangle$ is the mean force acting upon the element α at fixed $x_\alpha = \tilde{x}_\alpha^\sigma$ for the branch σ . In Fig. 22 (a) we show the two branches $\langle f \rangle_\sigma$ as a function of X_T for a system with parameters given in Tables 1 and 2. The transition from the F-UU states is the jump from one branch to the other.

²⁴By size we mean the length of the handles as well as the length or molecular weight of the RNA molecule. In general to apply the saddle point approximation we require that the energies of the different elements of the system (bead, handles and molecule) are several times $k_B T$.

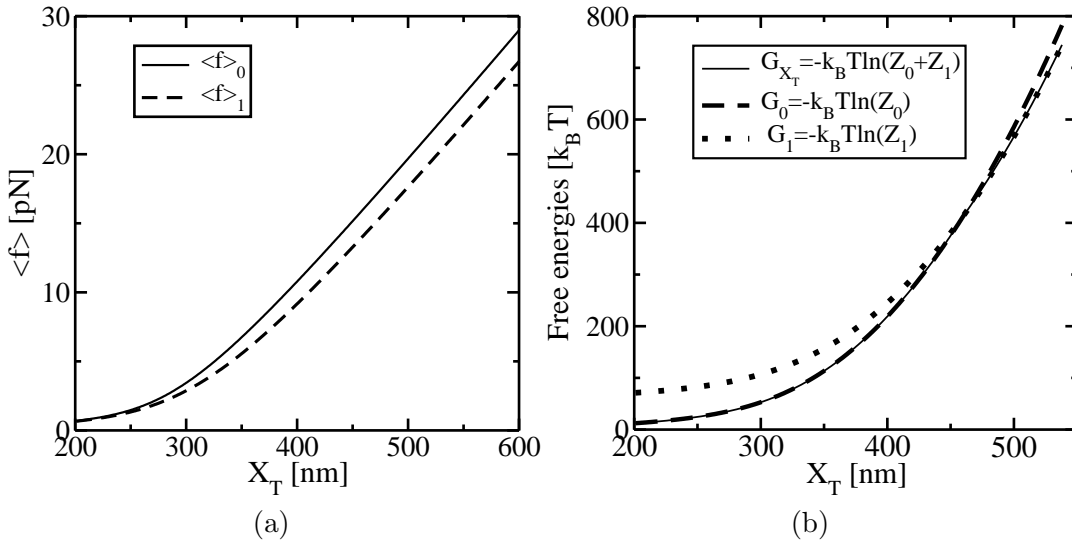


Figure 22: We consider a system with the parameters given in Tables 1 and 2. From the partition function analysis we compute: (a) The two branches $\langle f \rangle_\sigma$, corresponding to the thermodynamic forces acting upon the system for a given σ RNA state as a function of X_T . (b) The free energy G_{X_T} and the free energy of each branch σ , G_σ , as a function of X_T .

Hence we have obtained that the values of the arguments for which the contribution to the partition function is maximum corresponds to the equilibrium values at a given X_T :

$$Z(X_T) = Z_0(X_T) + Z_1(X_T) , \quad (\text{A-18})$$

$$Z_0(X_T) \approx \exp \left[-\beta (W_{h_1}(\langle x_{h_1} \rangle_0) + W_{h_2}(\langle x_{h_2} \rangle_0) + V_b(\langle x_b \rangle_0)) \right] , \quad (\text{A-19})$$

$$Z_1(X_T) \approx \exp \left[-\beta (W_{h_1}(\langle x_{h_1} \rangle_1) + W_{h_2}(\langle x_{h_2} \rangle_1) + V_b(\langle x_b \rangle_1) + \Delta G^0 + W_r(\langle x_r \rangle_1)) \right] . \quad (\text{A-20})$$

where we have neglect the subdominant contributions. The $\langle x_\alpha \rangle_\sigma$ correspond to the mean value of x_α for the branch σ and for a fixed value of X_T . In Fig. 22 (b) we show the results for the free energy of the system with parameters given in Tables 1 and 2 as a function of X_T ,

$$G_{X_T} = -k_B T \ln(Z(X_T)) , \quad (\text{A-21})$$

and also the free energies of the system for each branch σ ,

$$G_\sigma = -k_B T \ln(Z_\sigma(X_T)) . \quad (\text{A-22})$$

The free energy of the system G_{X_T} changes from one branch to the other at X_T^c , when both states are equal probable, i.e $G_0 = G_1$.

B Computation of the folding and unfolding rates in the mixed ensemble

We model the kinetics of the folding-unfolding of RNA as a Kramers activated process characterized by the following transitions rates:

$$\begin{aligned} k_{\rightarrow}(X_T) &= k_0 \exp[-\beta B(X_T)] \\ k_{\leftarrow}(X_T) &= k_0 \exp[\beta(-B(X_T) + \Delta G(X_T))] , \end{aligned} \quad (\text{B-1})$$

where k_0 is an attempt frequency that depends on the shape of the free energy landscape, on the molecular damping and on the natural frequency of the hydrogen bond oscillations [12]. The functions $\Delta G(X_T)$ and $B(X_T)$ are the difference of free energy between the F and UF states and the height of the kinetic barrier located between

them (Fig. 3 (a))²⁵. Using the results obtained from the partition function analysis we can write $\Delta G(X_T)$ as:

$$\Delta G(X_T) = -k_B T \ln \frac{Z_1(X_T)}{Z_0(X_T)} = \Delta G^0 + W_r(\langle x_r \rangle_1) - \langle f \rangle_0 x_m + \frac{1}{2} k_b x_m^2 + \Delta W_h , \quad (\text{B-2})$$

where we used (9,10) for the expressions of Z_0 and Z_1 and we used the parameter x_m defined as the distance between the two states, $x_m = \langle x \rangle_1 - \langle x \rangle_0$. The functions W_r and ΔW_h are given by (11) and (23).

The height of the barrier is given by the difference of free energy between the F state an the transition state that we will denote as $\sigma = t$ (averages taken when the molecule is in its transition state will be denoted by $\langle \dots \rangle_t$). The transition state is located at the point where the free energy landscape of the system depicted in Fig. 1 is maximum (Fig. 3 (a)), and we define it as the RNA state where the first n^* bases are opened and the latter $N - n^*$ are closed, N being the total number of bases that form the RNA molecule. Therefore the function $B(X_T)$ is computed as the free-energy difference between the folded state F and the transition state, which are separated by a distance $x_1 = \langle x \rangle_t - \langle x \rangle_0$. This gives

$$B(X_T) = B^0 + W_r(\langle x_r \rangle_t) - \langle f \rangle_0 x_1 + 1/2 k_b x_1^2 + \Delta W_h^t . \quad (\text{B-3})$$

The function W_r is given by (11) and ΔW_h^t is the change in free energy of the handles when the RNA molecule jumps from the F state to the transition state computed as:

$$\Delta W_h^t = W_{h1}(\langle x_{h1} \rangle_t) + W_{h2}(\langle x_{h2} \rangle_t) - W_{h1}(\langle x_{h1} \rangle_0) - W_{h2}(\langle x_{h2} \rangle_0) . \quad (\text{B-4})$$

Then the rates k_{\rightarrow} and k_{\leftarrow} associated to the activated process can be written as:

$$k_{\rightarrow}(X_T) = k_0 \exp[\beta(-B^1 + \langle f \rangle_0 x_1 - 1/2 k_b x_1^2)] , \quad (\text{B-5})$$

$$k_{\leftarrow}(X_T) = k_0 \exp[\beta(-B^1 + \Delta G^1 - \langle f \rangle_1 x_2 - 1/2 k_b x_2^2)] , \quad (\text{B-6})$$

$$\text{with } B^1 = B^0 + W_r(\langle x_r \rangle_t) + \Delta W_h^t , \quad \Delta G^1 = \Delta G^0 + W_r(\langle x_r \rangle_1) + \Delta W_h , \quad (\text{B-7})$$

where we used (B-1), (B-2) and (B-3). The expression for the rates (B-5,B-6) are equivalent to the ones obtained by Bell [31] but in the mixed ensemble. Note that the two rates $k_{\rightarrow}(X_T)$, $k_{\leftarrow}(X_T)$ satisfy the detailed balance condition (28).

C Demonstration of the equivalence between the N_F and N_B

Taking the expressions for the fractions N_F and N_R given by (29,30) and integrating the left integral we get:

$$\begin{aligned} N_F &= 1 - \rho_0^F(y_i, y_f) + \int_{y_i}^{y_f} \frac{d\rho_0^F(y_i, y)}{dy} \rho_1^F(y, y_f) dy , \\ N_R &= 1 - \rho_1^R(y_f, y_i) + \int_{y_f}^{y_i} \frac{d\rho_1^R(y_f, y)}{dy} \rho_0^R(y, y_i) dy , \end{aligned} \quad (\text{C-1})$$

where y denotes a generic control parameter. Then using the equation for the evolutions of the probabilities ρ_σ given by (31,32) and for a symmetric perturbation protocol, $v_F(y) = \frac{dy}{dt} \Big|_F = -v_R(y) = \frac{dy}{dt} \Big|_R$, we obtain the following relation:

$$\rho_\sigma^F(y', y) = \exp \left[- \int_{y'}^y \frac{k_{\sigma \rightarrow \sigma'}(y'')}{v_F(y'')} dy'' \right] = \exp \left[- \int_y^{y'} \frac{k_{\sigma \rightarrow \sigma'}(y'')}{v_R(y'')} dy'' \right] = \rho_\sigma^R(y, y') \quad (\text{C-2})$$

²⁵Note that the physical meaning of $\Delta G(X_T)$ is completely different from ΔG_{X_T} (see (15)). The latter corresponds to the free energy difference of the global system between two different values of X_T .

We consider the expression for N_R given by (C-1) and we integrate by parts,

$$N_R = 1 - \rho_1^R(y_f, y_i) - \rho_0^R(y_f, y_i) + \rho_1^R(y_f, y_i) - \int_{y_f}^{y_i} \frac{d\rho_0^R(y, y_i)}{dy} \rho_1^R(y_f, y) dy . \quad (\text{C-3})$$

Using the relation between the probabilities ρ_σ for the forward and reverse process (C-2), we obtain

$$N_R = 1 - \rho_0^F(y_i, y_f) + \int_{y_i}^{y_f} \frac{d\rho_0^F(y_i, y)}{dy} \rho_1^F(y, y_f) dy = N_F . \quad (\text{C-4})$$

D Single domain RNA as a stick-slip process

To address the case of a multidomain molecule it is useful to focus first on the simpler case of a single domain molecule. We consider an unfolding process without refolding ($k_{\leftarrow} = 0$) characterized by an effective unfolding force-dependent rate $k_{\rightarrow}(f)$ (33). The distribution of breakage forces is given by [12]

$$P(f^*) = \frac{k_{\rightarrow}(f^*) e^{-\frac{k_B T}{r \tilde{x}_1} [k_{\rightarrow}(f^*) - k_{\rightarrow}(0)]}}{r} . \quad (\text{D-1})$$

Note that in order to the no refolding condition to be realistic there must be a limit force f_m , below which the distribution of breakage forces goes to zero. This lower limit f_m arises because we are considering that there is a vanishing probability of jumping if the UF state is not thermodynamically stable, $\Delta G(f_m) = 0$. From this distribution one can compute the mean value and the variance of the breakage force [38, 23]

$$\langle f^* \rangle = \int_0^\infty df P(f) f = \frac{k_B T}{\tilde{x}_1} [-e^a Ei(-a)] , \quad (\text{D-2})$$

where $a = \frac{k_B T}{r \tilde{x}_1} k_{\rightarrow}(0)$ and the function Ei is the special elliptic function. By doing an expansion in the parameter a , that is much smaller than one (otherwise there is a finite probability of refolding), we obtain:

$$\langle f^* \rangle = \frac{k_B T}{\tilde{x}_1} \left[\ln \left(\frac{r \tilde{x}_1}{k_B T k_o e^{-(\tilde{B} - 1/2k_b \tilde{x}_1^2)}} \right) - \gamma \right] + O(a) . \quad (\text{D-3})$$

where γ is the Euler's constant, and

$$\sigma_{f^*}^2 = \langle f^{*2} \rangle - \langle f^* \rangle^2 = \left(\frac{k_B T}{\tilde{x}_1} \right)^2 [\pi^2/6] + O(a) . \quad (\text{D-4})$$

Therefore by studying either the distribution of f^* at fixed r or the mean value or the variance of such distribution as a function of r one can obtain information about the kinetic parameters doing a fit to (D-1), (D-3) or (D-4) respectively²⁶.

In Fig. 23 we plot $\langle f^* \rangle$ and $\sigma_{f^*}^2$ as a function of r obtained by pulling the system described in Sec. 2 with parameters given by Table 1. The kinetic parameters that characterize the RNA molecule that we consider here are given in Table 5.

$k_0 \exp(-\beta B^0)$	n^*
$e^{-9} \approx 10^{-4}$	2

Table 5: Parameters that characterize the unfolding kinetics of the RNA hairpin.

We perform two kinds of simulation both using the condition of no refolding (36), but with the dynamics generated by different unfolding rates, the non-effective rates (B-5) and the effective rates (33) respectively:

²⁶ The system under consideration verifies that the transition occurs close to the situation where the k_b is much smaller than the other stiffness values, k_{h_1} , k_{h_2} and k_r . Beyond this regime, one should take into account the variability of r with the force. And to get a more accurate result one should fit the data to the distribution of the breakage forces instead of the mean or variance of the breakage force as discussed in [37].

- Non-effective rates: We consider the explicit dependence on X_T of the barrier $B(X_T)$ that governs the unfolding kinetics, see (B-3).
- Effective rates: We use the unfolding effective rate (33) in order to generate the unfolding dynamics where we neglect the dependence on X_T of x_1 and B^1 as given by (B-7). For kinetics processes with barriers quite insensitive to the force (or X_T) this seems to be a reasonable approximation. The effective model is also the one we use to do the analytical computations.

The comparison between both simulations allows us to see how big are the difference between both models, and how far the analytical results are from the non-effective model. In Fig. 23 (b) we show $\sigma_{f^*}^2$ for both kinds of simulations for a broad range of values of r . The non-effective simulation gives fluctuations $\sigma_{f^*}^2$ that decrease when r increases, instead of being constant as the effective model predicts. This effect comes from the dependence of \tilde{x}_1 on f (or X_T). On the other hand we can see that when r approaches zero, fluctuations disappear, because the domain is always opened at zero force²⁷. However, we should note that in the latter regime (r going to zero) the no-refolding approximation becomes invalid, because the distribution $P(f^*)$ do not vanish for $f^* < f_m$. Nevertheless we see that for the range of interest $r \approx 1 - 50$ pN/s both simulations agree pretty well either for the $\sigma_{f^*}^2$ as for the $\langle f^* \rangle$. We can conclude that the effective dynamics reproduces well the non-effective one.

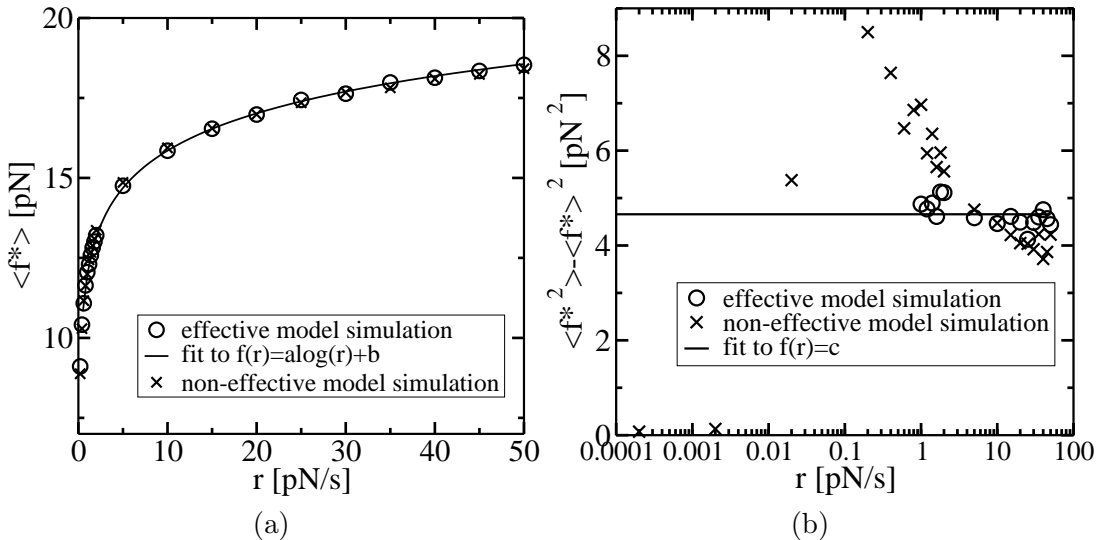


Figure 23: Comparison between the effective and non-effective rates. Results for 3000 pulling trajectories for a domain characterized by the kinetics parameters given in Table 5. For the effective kinetics parameters we use $\tilde{x}_1 = 2.5$ nm and $\tilde{B} \ln(k_o) = 8.5 k_B T$. In (a) it is shown the mean breakage force as a function of the pulling rate. The straight line is the best fit to a function $y = a \ln(x) + b$, obtaining $\tilde{x}_1 = 2.47 \pm 0.03$ nm, $\tilde{B} \ln(k_o) = 8.3 \pm 0.2 k_B T$. In (b) we represent the variance in breakage force as a function of the pulling rate. The straight line is the best fit to a constant $y = C$ for the data with $r > 1$ pN/s, obtaining $\tilde{x}_1 = 2.45 \pm 0.06$ nm.

Fitting the data obtained from the simulation for $\langle f^*(r) \rangle$ to (D-3), and for $\sigma_{f^*}^2$ to (D-4), we get accurate results for both parameters, \tilde{x}_1 and $\tilde{B} \ln(k_o)$.

E Computation of the distribution of probability of breakage force in regime 3

According to (D-1) the distribution of breakage forces for the i th domain conditioned to a given value of f_i^s (with $f_i^s = f_{i-1}^* - k_b \tilde{x}_m^{(i-1)}$), $\rho(f_i^* | f_i^s)$, is:

²⁷In the simulation there is no restriction for the breakage force, hence f^* can be smaller than f_m . When r goes to zero the breakage force too, because the molecule always opens if we wait long enough (and does not close anymore as $k_{\leftarrow} = 0$).

$$\rho(f_i^*|f_i^s) = \frac{k_{\rightarrow}^{(i)}(f_i^*) e^{\frac{k_B T}{r \tilde{x}_1^{(i)}} [k_{\rightarrow}^{(i)}(f_i^*) - k_{\rightarrow}^{(i)}(f_i^s)]}}{r} \theta_H(f_i^* - f_i^s) , \quad (\text{E-1})$$

where the parameters and functions with index i refer to the domain i . The θ_H is the Heaviside function, $\theta_H(x) = 1$ only if $x > 0$ otherwise $\theta_H(x) = 0$. Assuming $\tilde{x}_m^{(i-1)}$ as a constant parameter we derive the breakage force distribution $P(f_i^*)$ averaging (E-1) over the distribution of the breakage forces of the previous domain $i-1$, $P(f_{i-1}^*)$. To get $P(f_{i-1}^*)$ one has to average over the distribution of the breakage forces of the domain $i-2$, and so on. This leads to the following recurrence formula:

$$P(f_i^*) = C \int_{-\infty}^{\infty} \rho(f_i^*|f_i^s) \prod_{k=2}^{i-1} df_k^* \rho(f_k^*|f_k^s) df_k^* P(f_1^*) , \quad (\text{E-2})$$

where C is a normalization factor. We will consider the case where the distribution of breakage force for the domain $i-1$ is not modified by the previous one, either because it is the first domain, or because the typical value of f_{i-1}^* is higher than all the previous ones f_k^* with $k < i-1$. Then the distribution of f_{i-1}^* is computed as in the case of a single barrier (D-1) and (E-2) reduces to,

$$P(f_i^*) = C \int_{-\infty}^{\infty} \rho(f_i^*|f_i^s) P(f_{i-1}^*) df_{i-1}^* . \quad (\text{E-3})$$

The integral in (E-3) is not analytically solvable. Then we expand in power series the exponential $\exp\left[-\frac{k_B T}{r \tilde{x}_1^{(i)}} [k_{\rightarrow}^{(i)}(f_i^s)]\right]$ in (E-1) and substituting in (E-3) we obtain:

$$P(f_i^*) = C \frac{k_{\rightarrow}^{(i)}(f_i^*) e^{\frac{k_B T}{r \tilde{x}_1^{(i)}} k_{\rightarrow}^{(i)}(f_i^s)}}{r} \left[\sum_{j=0}^{\infty} \frac{A_i^j}{j!} \right] , \quad (\text{E-4})$$

where

$$\begin{aligned} A_i^j &= \int_{-\infty}^{f_i^* + k_b \tilde{x}_m^{(i-1)}} C_i P(f_{i-1}^*) df_{i-1}^* = \frac{[(k_B T / r \tilde{x}_1^{(i)}) k_{\rightarrow}^{(i)}(0) \exp(-\frac{k_b \tilde{x}_m^{(i-1)} \tilde{x}_1^{(i)}}{k_B T})]^j}{[(k_B T / r \tilde{x}_1^{(i-1)}) k_{\rightarrow}^{(i-1)}(0)]^{\tilde{x}_1^{(i)} j / \tilde{x}_1^{(i-1)}}} \\ &\times \gamma(j \tilde{x}_1^{(i)} / \tilde{x}_1^{(i-1)} + 1, \frac{k_B T}{r \tilde{x}_1^{(i-1)}} k_{\rightarrow}^{(i)}(f_i^* + k_b \tilde{x}_m^{(i-1)})) . \end{aligned} \quad (\text{E-5})$$

The $\gamma(x, y)$ is the incomplete gamma function. For the regime 3 the series can be truncated, because the moments of C_i , A_i^j , are not big and the series fastly converges.

References

- [1] J.A. Doudna and T.R. Cech, (2002) *Nature* **418**, 222-228
- [2] P.B. Moore and T.A. Steitz, (2002) *Nature* **418**, 229-235
- [3] C. Bustamante, J. Macosko and G. Wuire, (2000) *Nature Reviews, Molecular Cell Biology* **1**, 130-136
- [4] S. Smith, L. Finzi and C. Bustamante, (1992) *Science* **258**, 1122-1126.
- [5] S. Smith, Y. Cui and C. Bustamante, (1996) *Science* **271**, 795-799
- [6] P. Cluzel, A. Lebrun, C. Heller, R. Lavery, J.L. Viovy, D. Chatenay, D. and F. Caron, (1996) *Science* **271**, 792-794.
- [7] B. Essevaz-Roulet, U. Bockelmann and F. Heslot, (1997) *Proc. Natl. Acad. Sci. USA* **94**, 11935-11940.
- [8] R. Russell, X.W. Zhuang, H.P. Babcock, I.S. Millet, S. Doniach, S. Chu and D. Herschlag, (2002) *Proc. Natl. Acad. Sci. USA* **99**, 155-160
- [9] X.W. Zhuang, H. Kim, M.J.B. Pereira, H.P. Babcock, N.G. Walter and S. Chu, (2002) *Science* **296**, 1473-1476

- [10] D. Liphardt, B. Onoa, S. Smith, I. Tinoco and C. Bustamante, (2001) *Science* **292**, 733-737.
- [11] B. Onoa, D. Dumont, J. Liphardt, S. Smith, I. Tinoco and C. Bustamante, (2003) *Science* **299**, 1892-1895
- [12] E. Evans and K. Richie, (1997) *Biophys. J* **72**, 1541-1555
- [13] E. Evans and K. Richie, (1999) *Biophys. J* **76**, 2439-2447
- [14] S. Smith, Y. Cui and C. Bustamante, (2003), *Methods in Enzymology* **361**, 134-162.
- [15] D. Keller, D. Swigon and C. Bustamante, (2003) *Biophys. J.* **84**, 733-738
- [16] U. Gerland, R. Bundschuh and T. Hwa, (2003) *Biophys. J.* **84**, 2831-2840.
- [17] U. Gerland, R. Bundschuh and T. Hwa, (2001) *Biophys. J.* **81**, 1324-1332.
- [18] F. Ritort, C. Bustamante and I. Tinoco, (2002) *Proc. Natl. Acad. Sci. USA* **99**, 13544-13548.
- [19] J.M. Fernandez, S. Chu and A.F. Oberhauser, (2001) *Science* **292**, 653-654.
- [20] V. Muñoz, P.A. Thompson, J. Hofrichter and W.A. Eaton, (1997) *Nature* **390**, 196.
- [21] G. Bokinsky, D. Rueda, V.K. Misra, A. Gordus, M.M. Rhodes, H.P. Babcock, N.G. Walter and X. Zhuang, (2003) *Proc. Natl. Acad. Sci. USA* **100**, 9302-9307.
- [22] X.W. Zhuang, T. Ha, H.D. Kim, T. Centner, S. Labeit and S. Chu, (2000) *Proc. Natl. Acad. Sci. USA* **97**, 14241-14244
- [23] G. Hummer and A. Szabo, (2003) *Biophys. J.* **85**, 5-15
- [24] S. Cocco, R. Monasson and J. Marko, (2003) *Eur. Phys. J. E* **10**, 153
- [25] E. Marinari, A. Pagnani and F. Ricci-Tersenghi, (2002) *Phys. Rev. E* **65**, 041919
- [26] I. Tinoco and C. Bustamante, (2002) *Biophysical Chemistry* **102**, 513-533.
- [27] P.J. Flory, (1969) *Statistical mechanics of chain molecules*, appendix G, Oxford University Press (NY).
- [28] J.F. Marko and E.D Siggia, (1995) *Macromolecules* **28**, 8759-8770.
- [29] C. Bustamante, J.F. Marko, E.D. Siggia, and S. Smith, (1994) *Science* **265**, 1599-1600.
- [30] C. Bouchiat, M. Wang, J. Allemand, T. Strick, S. Block and V. Croquette, (1999) *Biophys. J.* **76**, 409-413.
- [31] I.G. Bell, (1978) *Science* **200**, 618-627
- [32] A. Imparato and L. Peliti, (2004) *EPJ*, PREPRINT
- [33] P. Zarrinkar and J. Williamson, (1994) *Science* **265**, 918-923.
- [34] X.W. Fang, P. Thiagarajan, T.R. Sosnick and T. Pan, (2002) *Proc. Natl. Acad. Sci. USA* **99**, 8518-8523.
- [35] R. Russell, I. Millet, M. Tate, L. Kwok, B. Nakatani, S. Gruner, S. Mochrie, V. Pande, S. Doniach, D. Herschlag and L. Pollak, (2002) *Proc. Natl. Acad. Sci. USA* **99**, 4266-4271.
- [36] X.W. Zuang, L.E. Bartley, H.P. Babcock, R. Russell, T.J. Ha, D. Herschlag and S. Chu, (2000) *Science* **288**, 2048-2051
- [37] C. Friedsam, A.K. Wehle, F. kühner, and H.E. Gaub, (2003) *J. Phys: Condens. Matter* **15**, S1709-S1723
- [38] C. Gerley, J.C. Voegel, P. Schaaf, B. Senger, M. Maaloum, J.K.H. Horber and J. Hemmerle, (2000) *Proc. Natl. Acad. Sci. USA* **97**, 10802-10807.
- [39] S. Harlepp, T. Marchal, J. Robert, J-F. Léger, A. Xayaphoummine, H. Isambert and D. Chatenay, (2003) *arXiv:physics/0309063 v1*
- [40] J. Liphardt, S. Dumont, S.B. Smith, I. Tinoco Jr. and C. Bustamante, (2002) *Science* **296**, 1832-1835.
- [41] F. Ritort, (2003) *Poincaré Seminar* **2**, 195-229. Preprint *arXiv:cond-mat/0401311*
- [42] P. G. Bolhuis, D. Chandler, C. Dellago and P. L. Geissler, (2002) *Ann. Rev. Phys. Chem.* **53**, 291-318.